NONLOCAL MICROPLANE CONCRETE MODEL WITH RATE EFFECT AND LOAD CYCLES. I: GENERAL FORMULATION

By Toshiaki Hasegawa[1] and Zdeněk P. Bažant,[2] Fellow, ASCE

ABSTRACT: The nonlocal microplane model for concrete is improved to describe unloading, reloading, cyclic loading, and the rate effect. The differences compared to the previous formulation are: (1) Normal strain component on the microplane is not split into its volumetric and deviatoric parts—rather the normal component is made dependent on the lateral normal strains on the microplane; and (2) instead of considering on each microplane only one shear strain vector parallel to the shear stress vector, the shear strain is represented by two independent components on the microplane. To introduce rate effect, the stress-strain law for each microplane component is described by a generalized Maxwell model—a series coupling of a linear viscous element and an elastoplastic-fracturing element. Nonlinear unloading-reloading hysteresis rules with back- and objective-stresses are developed to introduce hysteresis. The model is then combined with nonlocal theory to enable describing localization phenomena and avoid spurious mesh sensitivity due to strain softening. The numerical implementation in finite-element programs is described. The study consists of two parts; part I deals with the general formulation (part II deals with experimental verification).

INTRODUCTION

The heterogeneity of concretes and brittleness of its matrix are responsible for complex nonlinear triaxial behavior with strain-softening damage. To describe such behavior, many types of models for concrete have been developed and investigated. They may be grouped into two basic categories—the macroscopic phenomenologic models and the micromechanics-based models. The hypoelastic models, plasticity models, endochronic models, fracturing theory, and continuum damage mechanics models belong to the former category. The constitutive models in the second category are more limited at present. The microplane model is one effective model based on certain simplified micromechanics ideas. It has been proven to describe many experimentally observed features of concretes as well as rocks and soils (Bažant 1984; Bažant and Oh 1985; Bažant and Prat 1988; Bažant and Ožbolt 1990; Ožbolt and Bažant 1991; Carol et al. 1992). The microplane model has been combined with the nonlocal theory in order to make it applicable to localized fracture behavior and size effects, and to avoid spurious mesh sensitivity in finite element analysis (Bažant and Ožbolt 1990; Ožbolt and Bažant 1991).

The present study (Hasegawa and Bažant 1991) attempts to improve and generalize the previously developed microplane model in several respects, particularly with regard to response to cyclic loading as influenced by the loading rate. This influence is manifested in the shape and width of the hysteresis loops. The loading rate of course also strongly affects the response to monotonic loading.

It should be mentioned that another partly similar but in some basic aspects different model, with different advantages, was developed at Northwestern University (Ožbolt and Bažant 1991) at the same time as the model presented here. Because of scope limitations, a comparison of these two versions of the cyclic microplane model with rate effect is relegated to a subsequent study.

[1]Struct. Res. Engr., Shimizu Corp., 3-4-17 Etchujima, Koto-ku, Tokyo 135, Japan.
[2]Walter P. Murphy Prof. of Civ. Engrg., Northwestern Univ., 2145 Sheridan Rd., Evanston, IL 60208-3109.

Note. Discussion open until January 1, 1994. Separate discussions should be submitted for the individual papers in this symposium. To extend the closing date one month, a written request must be filed with the ASCE Manager of Journals. The manuscript for this paper was submitted for review and possible publication on September 23, 1991. This paper is part of the *Journal of Materials in Civil Engineering*, Vol. 5, No. 3, August, 1993. ©ASCE, ISSN 0899-1561/93/0003-0372/$1.00 + $.15 per page. Paper No. 2741.

MODIFICATION AND SIMPLIFICATION OF PREVIOUS MICROPLANE MODEL

A detailed description of the concept of microplane model and its evolution, beginning with the idea of Taylor (1938), was given in Bažant and Prat (1988) and is not repeated here. The following hypotheses, in some respects different from those used in the previous work, were adopted for the development of the present generalized cyclic and rate-dependent version of the model. (The Latin lower-case subscripts refer to Cartesian coordinates x_i, $i = 1, 2, 3$.)

Hypothesis I

The strains on any microplane are the resolved components of the macroscopic strain tensor ε_{ij} (this represents a tensorial kinematic constraint).

Hypothesis II

The microplane resists not only normal strains ε_N, but also in-plane shear-strain vectors (ε_{TK}, ε_{TM}), whose direction within each microplane is the same as that of the shear stress vector (σ_{TK}, σ_{TM}).

Hypothesis III

The normal-stress increments on a microplane depend on the resolved lateral strains ε_L on the same microplane.

Hypothesis IV

The inelastic shear-stress vector increment on each microplane depends on the resolved normal component of the macroscopic stress tensor σ_{ij} on the same microplane (this represents an additional static constraint).

Hypothesis V

Constitutive laws for the normal and shear components on the microplanes (microconstitutive law) are based on a generalized Maxwell rheologic model in which a linear viscous element is coupled in series with an elastoplastic-fracturing element.

Hypothesis VI

The microconstitutive laws for the normal and shear components on each microplane are mutually independent.

Hypothesis VI was justified in Bažant and Prat (1988). The decoupling of volumetric, deviatoric, and shear responses on the microplane seems at first an oversimplification. But success in the modeling of test data indicates that the appropriate coupling of the volumetric and deviatoric responses on the macroscopic level is obtained through the coupling of microplanes of all orientations due to the kinematic constraint. In contrast to the previous

formulations by Bažant and Prat (1988) and Carol et al. (1991), the normal microplane components are not split into volumetric and deviatoric parts in the present model.

According to hypothesis I, the normal-strain component and the strain vector components on a microplane of direction cosines n_i are

$$\varepsilon_N = n_j \varepsilon_j'' = n_j n_k \varepsilon_{jk} \quad \ldots\ldots (1a)$$

$$\varepsilon_{Ni} = n_i n_j n_k \varepsilon_{jk} \quad \ldots\ldots (1b)$$

In the previous microplane model, the shear-strain response was defined, for the sake of simplicity, only in terms of magnitudes $\varepsilon_T = \sqrt{\varepsilon_{Ti}\varepsilon_{Ti}} = [n_k \varepsilon_{jm} n_m (\varepsilon_{jk} - n_i n_j \varepsilon_{ik})]^{1/2}$. With this definition, the strain magnitudes are always positive. But this makes it is impossible to describe the cyclic response on microplanes. To avoid this limitation, two in-plane unit coordinate vectors **k** and **m**, normal to each other, are introduced on each microplane as shown in Fig. 1(*b*), and two shear components ε_{TK}, ε_{TM} in those directions

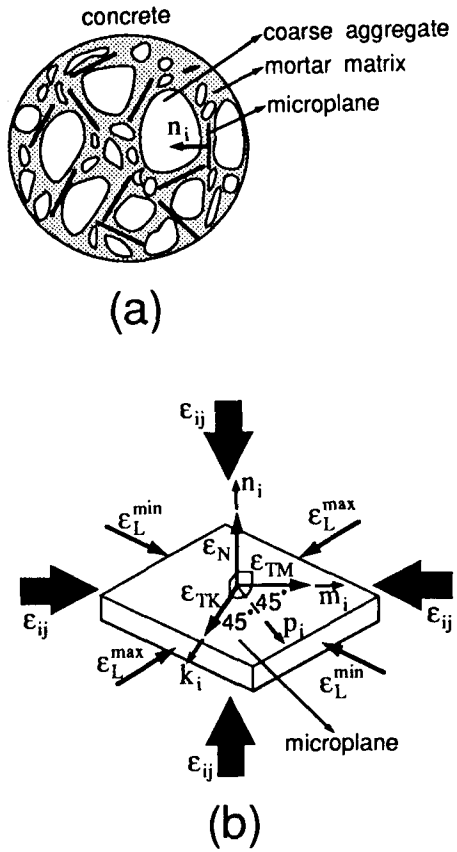

FIG. 1. (*a*) Microplanes in Concrete; (*b*) Unit Vectors n, k, m; and p on Microplane; (c) Microplane System (without Shear Response) and Generalized Maxwell Model for Each Microplane; (*d*) Numerical Integration Points on Unit Hemisphere for 21 Integration Points Formula

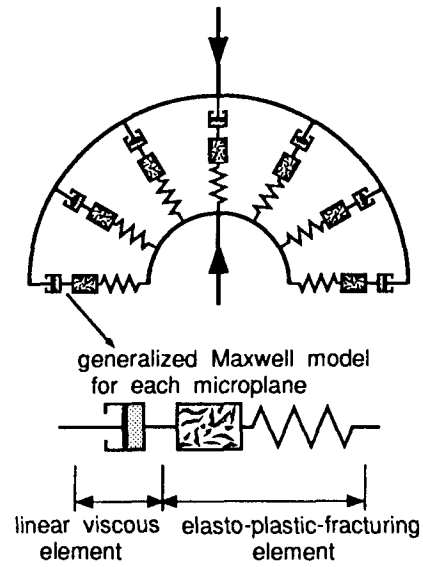

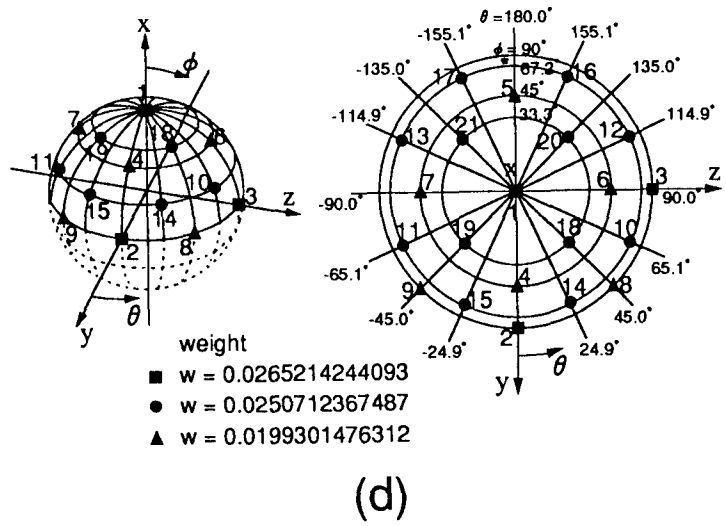

FIG. 1. (*Continued*)

are considered. Since the directions of the vector **k** and **m** must be fixed at the beginning of calculations, some kind of rule to determine these directions is necessary. The rule must not have a significant bias for any direction; i.e., the frequency of various directions within the microplanes taken by vectors **m** and **n** must be about the same. This is approximately achieved by the following simple rule: vector **m** of microplane 1 is determined to be

normal to the z-axis, vector $\mathbf{m}$ of microplane 2 normal to the x-axis, vector $\mathbf{m}$ of microplane 3 normal to the y-axis, vector $\mathbf{m}$ of microplane 4 normal again to the z-axis, and so on. Then for vector $\mathbf{m}$ normal to z-axis

$$m_1 = \frac{n_2}{\sqrt{n_1^2 + n_2^2}}; \qquad m_2 = \frac{-n_1}{\sqrt{n_1^2 + n_2^2}}; \qquad m_3 = 0 \quad \ldots\ldots\ldots\ldots (2a)$$

but $m_1 = 1$; $m_2 = 0$; $m_3 = 0$ if $n_1 = n_2 = 0$.

For vector $\mathbf{m}$ normal to x-axis

$$m_2 = \frac{n_3}{\sqrt{n_2^2 + n_3^2}}; \qquad m_3 = \frac{-n_2}{\sqrt{n_2^2 + n_3^2}}; \qquad m_1 = 0 \quad \ldots\ldots\ldots\ldots (2b)$$

but $m_1 = 0$; $m_2 = 1$; $m_3 = 0$ if $n_2 = n_3 = 0$.

For vector $\mathbf{m}$ normal to y axis

$$m_1 = \frac{-n_3}{\sqrt{n_1^2 + n_3^2}}; \qquad m_3 = \frac{n_1}{\sqrt{n_1^2 + n_3^2}}; \qquad m_2 = 0 \quad \ldots\ldots\ldots\ldots (2b)$$

but $m_1 = 0$; $m_2 = 0$; $m_3 = 1$ if $n_1 = n_3 = 0$.

After determining vector $\mathbf{m}$, vector $\mathbf{k}$ is calculated for each microplane as $\mathbf{k} = \mathbf{m} \times \mathbf{n}$. According to hypothesis II, the in-plane shear strain components in the $\mathbf{k}$ and $\mathbf{m}$ directions on a microplane of direction cosines n_i are

$$\varepsilon_{TK} = k_j \varepsilon_j^n = k_j n_i \varepsilon_{ij} = \frac{1}{2}(k_i n_j + k_j n_i)\varepsilon_{ij} \quad \ldots\ldots\ldots\ldots (3a)$$

$$\varepsilon_{TM} = m_j \varepsilon_j^n = m_j n_i \varepsilon_{ij} = \frac{1}{2}(m_i n_j + m_j n_i)\varepsilon_{ij} \quad \ldots\ldots\ldots\ldots (3b)$$

where symmetry of ε_{ij} was exploited to symmetrize these expressions. The separate treatment of ε_{TK} and ε_{TM} brings about an improvement over the previous microplane formulation by Bažant and Prat (1988), but it increases the number of variables.

INCREMENTAL MACROSCOPIC STRESS-STRAIN RELATIONSHIP

The incremental microconstitutive relations are written separately for the normal component and the shear components in the K and M directions

$$d\sigma_N = C_N\, d\varepsilon_N - d\sigma''_N \qquad \text{for normal component} \quad \ldots\ldots\ldots\ldots (4a)$$

$$d\sigma_{TK} = C_{TK}\, d\varepsilon_{TK} - d\sigma''_{TK} \qquad \text{for } K\text{-shear component} \quad \ldots\ldots\ldots\ldots (4b)$$

$$d\sigma_{TM} = C_{TM}\, d\varepsilon_{TM} - d\sigma''_{TM} \qquad \text{for } M\text{-shear component} \quad \ldots\ldots\ldots\ldots (4c)$$

in which $d\sigma_N$, $d\sigma_{TK}$, and $d\sigma_{TM}$ = incremental microstresses; C_N, C_{TK}, and C_{TM} = incremental elastic stiffnesses; and $d\sigma''_N$, $d\sigma''_{TK}$, and $d\sigma''_{TM}$ = inelastic microstress increments. Note that there is no coupling between K-shear and M-shear (decoupling hypothesis for shear).

Using the principle of virtual work (i.e., equality of virtual works of the macrostresses and microstresses), we can write

$$\frac{4\pi}{3}\, d\sigma_{ij}\delta\varepsilon_{ij} = 2\int_S (d\sigma_N \delta\varepsilon_N + d\sigma_{TK}\delta\varepsilon_{TK} + d\sigma_{TM}\delta\varepsilon_{TM}) f(\mathbf{n})\, dS \quad \ldots\ldots (5)$$

in which $\delta\varepsilon_{ij}$, $\delta\varepsilon_N$, $\delta\varepsilon_{TK}$, and $\delta\varepsilon_{TM}$ = small variations of the macroscopic strain tensor and of the microstrain components on a microplane. The constant $4\pi/3$ means that the macroscopic work is taken over the volume of a unit sphere. The factor 2 on the right-hand side arises because the microscopic work needs to be integrated only over the surface of a unit hemisphere S. The function $f(\mathbf{n})$ is a weight function for the normal directions $\mathbf{n}$, which in general can introduce anisotropy of the material in its initial state. We will use $f(\mathbf{n}) = 1$, which means isotropy. Expressing $\delta\varepsilon_N$, $\delta\varepsilon_{TK}$, and $\delta\varepsilon_{TM}$ from (1) and (3) and substituting them into (5), we can get

$$\frac{4\pi}{3}\, d\sigma_{ij}\delta\varepsilon_{ij} = 2\int_S \left[n_i n_j\, d\sigma_N + \frac{d\sigma_{TK}}{2}(k_i n_j + k_j n_i) + \frac{d\sigma_{TM}}{2}(m_i n_j + m_j n_i)\right] f(\mathbf{n})\, dS\delta\varepsilon_{ij} \quad \ldots\ldots (6)$$

This variational equation must hold for any variations $\delta\varepsilon_{ij}$; therefore we can delete $\delta\varepsilon_{ij}$; and substituting (4) we obtain

$$d\sigma_{ij} = \frac{3}{2\pi}\int_S \left[n_i n_j\, d\sigma_N + \frac{d\sigma_{TK}}{2}(k_i n_j + k_j n_i) + \frac{d\sigma_{TM}}{2}(m_i n_j + m_j n_i)\right] f(\mathbf{n})\, dS \quad \ldots\ldots (7a)$$

$$d\sigma_{ij} = \frac{3}{2\pi}\int_S \left[n_i n_j (C_N\, d\varepsilon_N - d\sigma''_N) + \frac{1}{2}(k_i n_j + k_j n_i)(C_{TK}\, d\varepsilon_{TK} - d\sigma''_{TK}) + \frac{1}{2}(m_i n_j + m_j n_i)(C_{TM}\, d\varepsilon_{TM} - d\sigma''_{TM})\right] f(\mathbf{n})\, dS \quad \ldots\ldots (7b)$$

Eqs. (1) and (3) may now be here substituted for ε_N, ε_{TK}, and ε_{TM}. This finally yields the macroscopic incremental stress-strain relation

$$d\sigma_{ij} = C_{ijrs}\, d\varepsilon_{rs} - d\sigma''_{ij} \quad \ldots\ldots\ldots\ldots (8)$$

in which C_{ijrs} denotes the incremental elastic stiffness tensor

$$C_{ijrs} = \frac{3}{2\pi}\int_S \left[n_i n_j n_r n_s C_N + \frac{1}{4}(k_i n_j + k_j n_i)(k_r n_s + k_s n_r) C_{TK} + \frac{1}{4}(m_i n_j + m_j n_i)(m_r n_s + m_s n_r) C_{TM}\right] f(\mathbf{n})\, dS \quad \ldots\ldots (9)$$

and $d\sigma''_{ij}$ denotes the inelastic stress increments

$$d\sigma''_{ij} = \frac{3}{2\pi}\int_S \left[n_i n_j\, d\sigma''_N + \frac{1}{2}(k_i n_j + k_j n_i)\, d\sigma''_{TK} + \frac{1}{2}(m_i n_j + m_j n_i)\, d\sigma''_{TM}\right] f(\mathbf{n})\, dS \quad \ldots\ldots (10)$$

For the initial isotropic elastic response we can substitute the initial moduli C_N^0 and C_T^0 for C_N and C_{TK}, C_{TM} in (9), and set $f(\mathbf{n}) = 1$. Since these moduli are independent of the microplane direction, we could integrate (9) explicitly

if the unit vectors **k** and **m** were also known explicitly. However, they are not explicit, being calculated numerically as described before.

For initial elasticity we can substitute the initial moduli C_N^0 and C_T^0 for C_N and C_{TK}, C_{TM} in (4), and set $d\sigma''_N = d\sigma''_{TK} = d\sigma''_{TM} = 0$. Then we have $d\sigma_{TK} = C_T^0\, d\varepsilon_{TK}$ and $d\sigma_{TM} = C_T^0\, d\varepsilon_{TM}$ for shears. From that, $|d\boldsymbol{\sigma}_T| = C_T^0 |d\boldsymbol{\varepsilon}_T|$, where $|d\boldsymbol{\sigma}_T| = \sqrt{d\sigma_{TK}^2 + d\sigma_{TM}^2}$ and $|d\boldsymbol{\varepsilon}_T| = \sqrt{d\varepsilon_{TK}^2 + d\varepsilon_{TM}^2}$. This is the same relation as that used in the previous microplane model involving normal and shear components (Bažant 1984) (in which the shear vectors were characterized by three components in the Cartesian coordinates x_i; $i = 1, 2, 3$). Therefore the expressions derived in that study apply

$$C_N^0 = \frac{E}{(1 - 2\nu)} \qquad (11a)$$

$$C_T^0 = \frac{(1 - 4\nu)E}{(1 - 2\nu)(1 + \nu)} \qquad (11b)$$

in which E and ν = Young's modulus and Poisson's ratio.

One can now realize from (11) that only Poisson's ratios ν within the range $-1 \le \nu \le 0.25$ can be obtained with the present microplane model, while the microplane model with separate volumetric, deviatoric, and shear components (Bažant and Prat 1988) can describe elastic behavior with any thermodynamically possible Poisson's ratio $-1 \le \nu \le 0.5$. However, the disadvantage of the limited range of Poisson's ratio in the present model does not seem very serious for concrete, since for usual concretes $0.15 \le \nu \le 0.22$. In general, of course, we do not advocate abandoning the previous formulation with the full range of ν, which is in principle more realistic. The present restriction on the range of ν is due to avoiding a split of normal microplane components into volumetric and deviatoric ones, which brings about a simplification of the formulation.

RHEOLOGIC MODEL FOR RATE EFFECT IN MICROCONSTITUTIVE LAW

For cyclic behavior it is important to specify appropriate rate-dependent microconstitutive models. In this study a series coupling of a linear viscous element and an elastoplastic-fracturing element is adopted for the microconstitutive law on each microplane [Fig. 1(*c*)]. For the sake of brevity of notation, let ε and σ now represent any of the microstrains ε_N, ε_{TK}, and ε_{TM} and microstresses σ_N, σ_{TK}, and σ_{TM}. The model is described by the differential equation

$$\frac{d\sigma}{dt} = C^t \frac{d\varepsilon}{dt} - \frac{\sigma}{\rho} \qquad (12)$$

where $C^t = C^v$ for virgin loading; $C^t = C^{ur}$ for unloading and reloading; t = time; ρ = relaxation time of the viscous element; and C^t = current tangential stiffness of the elastoplastic-fracturing element, which takes the value of either C^v or C^{ur} depending on the loading-unloading-reloading criteria described later. When (12) is solved by using a central difference approximation, numerical difficulties or instabilities may be encountered in the case of strain softening, and even if the solution is numerically stable, a large error is usually accumulated and the stress is not reduced exactly to zero at very large strains.

To avoid these difficulties, the exponential algorithm, initially developed for aging creep of concrete (Bažant 1971, 1988), is applied in this study in a similar way as in an alternative nonlocal microplane model of Bažant and Ožbolt (1990). To achieve unrestricted numerical stability, we need to rewrite (12) so that it involves a positive incremental stiffness or unload-reload stiffness throughout the entire range of hardening and softening

$$\frac{d\sigma}{dt} = C^{ur} \frac{d\varepsilon}{dt} - \frac{\sigma}{\beta} \qquad (13)$$

$$\frac{1}{\beta} = \frac{1}{\rho} + (C^{ur} - C^t)\sigma \frac{d\varepsilon}{dt} \qquad (14)$$

in which β = a quasi-relaxation time for the purpose of calculation. When we apply (13) and (14) to finite steps, it is most accurate to take the values of C^{ur}, C^t, ρ, and σ for the middle of the time step (t_r, t_{r+1}), denoted with subscript $r + 1/2$, in which r = number of the step ($r = 1, 2, \ldots$)

$$\frac{d\sigma}{dt} = C^{ur}_{r+1/2} \frac{d\varepsilon}{dt} - \frac{\sigma}{\beta_{r+1/2}} \qquad (15)$$

$$\frac{1}{\beta_{r+1/2}} = \frac{1}{\rho_{r+1/2}} + (C^{ur}_{r+1/2} - C^t_{r+1/2})\sigma_{r+1/2} \frac{\Delta\varepsilon}{\Delta t} \qquad (16)$$

$C^{ur}_{r+1/2}$ and $\beta_{r+1/2}$ in these equations are assumed to be constant for the duration of each time step; however, to calculate $\sigma_{r+1/2}$, $C^{ur}_{r+1/2}$, and $C^t_{r+1/2}$, we need σ_{r+1}, C^{ur}_{r+1}, and C^t_{r+1}, which means that numerical iterations of the time step are necessary. The general solution of (15) is then exactly

$$\sigma(t) = Ae^{-(t-t_r)/\beta_{r+1/2}} + C^{ur}_{r+1/2}\beta_{r+1/2} \frac{d\varepsilon}{dt} \qquad (17)$$

in which A = an integration constant. From the initial condition $\sigma = \sigma_r$ at $t = t_r$, the integration constant can be calculated as $A = \sigma_r - C^{ur}_{r+1/2}\beta_{r+1/2}\, d\varepsilon/dt$, and then

$$\sigma(t) = \sigma_r e^{-(t-t_r)/\beta_{r+1/2}} + [1 - e^{-(t-t_r)/\beta_{r+1/2}}] C^{ur}_{r+1/2}\beta_{r+1/2} \frac{d\varepsilon}{dt} \qquad (18)$$

For the end of the time step, $t = t_{r+1} = t_r + \Delta t$, we have

$$\sigma_r + \Delta\sigma = \sigma_r e^{-\Delta z} + \frac{1}{\Delta z}(1 - e^{-\Delta z}) C^{ur}_{r+1/2}\Delta\varepsilon \qquad (19)$$

where $\Delta z = \Delta t/\beta_{r+1/2}$. We can rewrite (19) in the form of (4)

$$\Delta\sigma = \frac{1}{\Delta z}(1 - e^{-\Delta z}) C^{ur}_{r+1/2}\Delta\varepsilon - (1 - e^{-\Delta z})\sigma_r = C\Delta\varepsilon - \Delta\sigma'' \qquad (20)$$

where

$$C = \frac{1}{\Delta z}(1 - e^{-\Delta z}) C^{ur}_{r+1/2} \qquad (21)$$

$$\Delta\sigma'' = (1 - e^{-\Delta z})\sigma_r \qquad (22)$$

MICROCONSTITUTIVE LAW FOR NORMAL COMPONENTS

To be able to model the response to hydrostatic pressure, we must assume the stress-strain curve for the normal component to be the same as for the volumetric component of the previous microplane model. But then reasonable postpeak strain-softening would not be obtained for uniaxial or biaxial compression. This problem is circumvented by hypothesis III. The purpose of including a dependence on lateral strains is to achieve the following: (1) The normal strain response would not be the same as the volumetric or hydrostatic response except when the lateral strains are the same as the normal strain, which is the case of hydrostatic loading; while at the same time (2) the normal response would be more brittle when the difference between the normal and lateral strains is large, i.e., it would exhibit more strain softening.

To implement hypothesis III, we need to derive equations for the maximum and minimum principal values $\varepsilon_L^{\max}$, $\varepsilon_L^{\min}$ of lateral strain on each microplane. To this end we introduce another in-plane unit vector $\mathbf{p}$, whose angle with the unit vectors $\mathbf{k}$ and $\mathbf{m}$ is 45°, as shown in Fig. 1(*b*); $\mathbf{p} = (\mathbf{k} + \mathbf{m})/\sqrt{2}$. The lateral normal strains in the directions of $\mathbf{k}$, $\mathbf{m}$, and $\mathbf{p}$ are

$$\varepsilon_K = k_i k_j \varepsilon_{ij} \quad \ldots\ldots (23a)$$

$$\varepsilon_M = m_i m_j \varepsilon_{ij} \quad \ldots\ldots (23b)$$

$$\varepsilon_P = p_i p_j \varepsilon_{ij} \quad \ldots\ldots (23c)$$

Considering Mohr's circle for in-plane strains in the microplane, we can get the maximum and minimum principal values $\varepsilon_L^{\max}$, $\varepsilon_L^{\min}$ of the lateral strain on each microplane

$$\varepsilon_L^{\max} = \frac{\varepsilon_K + \varepsilon_M}{2} + \sqrt{\left(\frac{\varepsilon_K - \varepsilon_M}{2}\right)^2 + \left(\frac{\varepsilon_K + \varepsilon_M}{2} - \varepsilon_P\right)^2} \quad \ldots\ldots (24)$$

$$\varepsilon_L^{\min} = \frac{\varepsilon_K + \varepsilon_M}{2} - \sqrt{\left(\frac{\varepsilon_K - \varepsilon_M}{2}\right)^2 + \left(\frac{\varepsilon_K + \varepsilon_M}{2} - \varepsilon_P\right)^2} \quad \ldots\ldots (25)$$

which are invariant. It is useful to define a lateral-deviatoric strain ε_{LD} that combines $\varepsilon_L^{\max}$ and $\varepsilon_L^{\min}$ into one strain invariant for the microplane

$$\varepsilon_{LD} = |\varepsilon_N - \varepsilon_L^{\max}| + |\varepsilon_N - \varepsilon_L^{\min}| \quad \ldots\ldots (26)$$

To be able to change the normal response from the hydrostatic stress-strain response, which always has a positive slope, to plastic response (zero slope) and softening response (negative slope), the following hardening-softening function $\phi(\varepsilon_{LD})$ in terms of ε_{LD} may be introduced [Fig. 2(*b*)]:

$$\phi(\varepsilon_{LD}) = \frac{1}{1 + \left(\dfrac{\varepsilon_{LD}}{\varepsilon_{LD}^1}\right)^m} \quad \ldots\ldots (27a)$$

$$\phi(\varepsilon_{LD}) = \phi^p \quad \text{when } \varepsilon_{LD} = \varepsilon_{LD}^p \quad \ldots\ldots (27b)$$

$$\phi(\varepsilon_{LD}) = 0 \quad \text{when } \varepsilon_L^{\max} > 0 \quad \ldots\ldots (27c)$$

in which $\varepsilon_{LD}^1 = \varepsilon_{LD}$ value when $\phi(\varepsilon_{LD}) = 0.5$; m = a constant that specifies

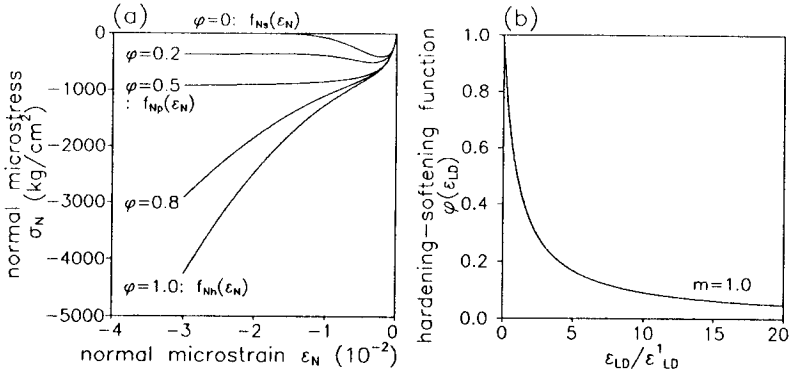

FIG. 2. (*a*) Dependence of Normal Compression Microstress-Strain Curve on Lateral Strain; (*b*) Hardening-Softening Function for Normal Compression

the shape of the curve $\phi(\varepsilon_{LD})$; and ϕ^p = value corresponding to the case of plastic response.

Now we try to set weight functions in terms of $\phi(\varepsilon_{LD})$ and use them to obtain a gradual transition from hydrostatic response to plastic response and softening response for the virgin loading curve of the normal-strain component of the microplane; for $0 \le \varepsilon_{LD} \le \varepsilon_{LD}^p$

$$\sigma_N(\varepsilon_N, \varepsilon_{LD}) = \left(\frac{\phi(\varepsilon_{LD}) - \phi^p}{1 - \phi^p}\right) f_{Nh}(\varepsilon_N) + \left(\frac{1 - \phi(\varepsilon_{LD})}{1 - \phi^p}\right) f_{Np}(\varepsilon_N) \quad \ldots (28a)$$

For $\varepsilon_{LD}^p < \varepsilon_{LD}$

$$\sigma_N(\varepsilon_N, \varepsilon_{LD}) = \left(\frac{\phi(\varepsilon_{LD})}{\phi^p}\right) f_{Np}(\varepsilon_N) + \left(\frac{\phi^p - \phi(\varepsilon_{LD})}{\phi^p}\right) f_{Ns}(\varepsilon_N) \quad \ldots\ldots (28b)$$

in which $f_{Nh}(\varepsilon_N)$ = hydrostatic loading curve of normal component when $\varepsilon_{LD} = 0$; $f_{NP}(\varepsilon_N)$ = plastic loading curve of normal component when $\varepsilon_{LD} = \varepsilon_{LD}^p$; and $f_{Ns}(\varepsilon_N)$ = softening loading curve of normal component when $\varepsilon_{LD} = \infty$ [Fig. 2(*a*)].

To obtain the loading tangential stiffness, we need to differentiate (28); for $0 \le \varepsilon_{LD} \le \varepsilon_{LD}^p$

$$\frac{d\sigma_N(\varepsilon_N, \varepsilon_{LD})}{d\varepsilon_N} = \left(\frac{\phi(\varepsilon_{LD}) - \phi^p}{1 - \phi^p}\right) \frac{df_{Nh}(\varepsilon_N)}{d\varepsilon_N} + \left(\frac{1 - \phi(\varepsilon_{LD})}{1 - \phi^p}\right) \frac{df_{Np}(\varepsilon_N)}{d\varepsilon_N} \quad \ldots\ldots (29a)$$

For $\varepsilon_{LD}^p < \varepsilon_{LD}$

$$\frac{d\sigma_N(\varepsilon_N, \varepsilon_{LD})}{d\varepsilon_N} = \left(\frac{\phi(\varepsilon_{LD})}{\phi^p}\right) \frac{df_{Np}(\varepsilon_N)}{d\varepsilon_N} + \left(\frac{\phi^p - \phi(\varepsilon_{LD})}{\phi^p}\right) \frac{df_{Ns}(\varepsilon_N)}{d\varepsilon_N} \quad \ldots (29b)$$

Similarly, the transition for the linear unload-reload stiffnesses C_N^{ur0} $(\sigma_N^u, \varepsilon_N^u, \varepsilon_{LD})$ may be written as follows; for $0 \le \varepsilon_{LD} \le \varepsilon_{LD}^p$

$$C_N^{ur0}(\sigma_N^u, \varepsilon_N^u, \varepsilon_{LD}) = \left(\frac{\phi(\varepsilon_{LD}) - \phi^p}{1 - \phi^p}\right) C_{Nh}^{ur0}(\sigma_N^u, \varepsilon_N^u)$$

$$+ \left(\frac{1 - \phi(\varepsilon_{LD})}{1 - \phi^p} \right) C_{Np}^{ur0}(\sigma_N^u, \varepsilon_N^u) \quad \ldots\ldots\ldots\ldots\ldots\ldots\ldots\ldots\ldots\ldots (30a)$$

For $\varepsilon_{LD}^p < \varepsilon_{LD}$

$$C_N^{ur0}(\sigma_N^u, \varepsilon_N^u, \varepsilon_{LD}) = \left(\frac{\phi(\varepsilon_{LD})}{\phi^p} \right) C_{Np}^{ur0}(\sigma_N^u, \varepsilon_N^u)$$

$$+ \left(\frac{\phi^p - \phi(\varepsilon_{LD})}{\phi^p} \right) C_{Ns}^{ur0}(\sigma_N^u, \varepsilon_N^u) \quad \ldots\ldots\ldots\ldots\ldots\ldots\ldots\ldots\ldots\ldots (30b)$$

in which $C_{Nh}^{ur0}(\sigma_N^u, \varepsilon_N^u)$ = hydrostatic linear unload-reload stiffness of the normal component when $\varepsilon_{LD} = 0$; $C_{Np}^{ur0}(\sigma_N^u, \varepsilon_N^u)$ = plastic linear unload-reload stiffness of the normal component when $\varepsilon_{LD} = \varepsilon_{LD}^p$; $C_{Ns}^{ur0}(\sigma_N^u, \varepsilon_N^u)$ = softening linear unload-reload stiffness of the normal component when $\varepsilon_{LD} = \infty$; σ_N^u and ε_N^u = stress and strain at the start of unloading.

In the previous microplane model, virgin loading curves for strain-softening on each microplane were formulated using a single exponential function, $\sigma = C^0 e^{-|\varepsilon/a|^{-p}}\varepsilon$. With this kind of equation, however, one cannot adjust the peak stress, peak strain, and postpeak ductility individually. It is more versatile to introduce equations that can do so. Therefore, in this study the following virgin loading curves are used for pre- and postpeak tensile regions of the normal component [Fig. 3(*a*)].

For $0 \leq \varepsilon_N \leq \varepsilon_{NT}^0$ (prepeak)

$$\sigma_N = \sigma_{NT}^0 \left[1 - \left(1 - \frac{\varepsilon_N}{\varepsilon_{NT}^0} \right)^{C_N^0 \varepsilon_{NT}^0 / \sigma_{NT}^0} \right] \quad \text{with } \varepsilon_{NT}^0 = \frac{\sigma_{NT}^0}{\zeta_{NT} C_N^0} \quad \ldots\ldots (31a)$$

For $\varepsilon_{NT}^0 < \varepsilon_N$ (postpeak)

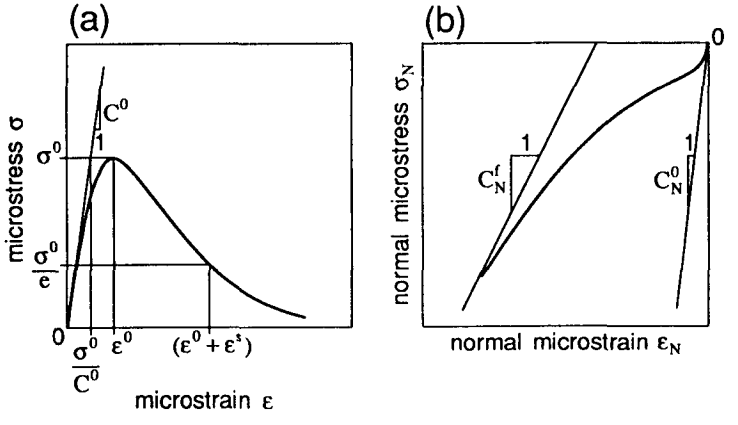

FIG. 3. (a) Strain-Softening Curve for Microplane; (*b*) Hydrostatic Curve for Normal Compression

$$\sigma_N = \sigma_{NT}^0 \exp\left[- \left(\frac{\varepsilon_N - \varepsilon_{NT}^0}{\varepsilon_{NT}^s} \right)^{p_{NT}} \right] \quad \text{with } \varepsilon_{NT}^s = \gamma_{NT}\varepsilon_{NT}^0 = \frac{\gamma_{NT}\sigma_{NT}^0}{\zeta_{NT} C_N^0}$$
$$\ldots\ldots\ldots\ldots\ldots\ldots\ldots\ldots\ldots\ldots\ldots\ldots\ldots\ldots\ldots\ldots\ldots\ldots\ldots\ldots\ldots\ldots (31b)$$

In (31), σ_{NT}^0 = peak stress of the curve; ζ_{NT} = a parameter that controls the peak strain ε_{NT}^0; and γ_{NT} = a parameter that controls ε_{NT}^s. At the strain $\varepsilon_N = \varepsilon_{NT}^0 + \varepsilon_{NT}^s$, the stress decreases to σ_{NT}^0/e in the softening region; p_{NT} = a parameter that changes the shape of the softening curve. Thus we can control the shape of the stress-strain curve with these four parameters quite easily, which is important for being able to adjust properly the macroscopic response with the microplane model; C_N^0 = initial modulus for the normal component, which can be determined from (11).

For the compression range of the normal component, we must specify the equations for softening, plastic, and hydrostatic stress-strain curves, as mentioned before. The same types of equation as for tension are assumed as for compression softening of the normal component [Fig. 3(*a*)].

For $0 \geq \varepsilon_N \geq \varepsilon_{NC}^0$ (prepeak)

$$f_{Ns}(\varepsilon_N) = \sigma_N = \sigma_{NC}^0 \left[1 - \left(1 - \frac{\varepsilon_N}{\varepsilon_{NC}^0} \right)^{C_N^0 \varepsilon_{NC}^0 / \sigma_{NC}^0} \right]$$

$$\text{with } \varepsilon_{NC}^0 = \frac{\sigma_{NC}^0}{\zeta_{NC} C_N^0} \quad \ldots\ldots\ldots\ldots\ldots\ldots\ldots\ldots\ldots\ldots\ldots\ldots\ldots\ldots\ldots\ldots (32a)$$

for $\varepsilon_{NC}^0 > \varepsilon_N$ (postpeak)

$$f_{Ns}(\varepsilon_N) = \sigma_N = \sigma_{NC}^0 \exp\left[- \left(\frac{\varepsilon_N - \varepsilon_{NC}^0}{\varepsilon_{NC}^s} \right)^{p_{NC}} \right]$$

$$\text{with } \varepsilon_{NC}^s = \gamma_{NC}\varepsilon_{NC}^0 = \frac{\gamma_{NC}\sigma_{NC}^0}{\zeta_{NC} C_N^0} \quad \ldots\ldots\ldots\ldots\ldots\ldots\ldots\ldots\ldots\ldots\ldots\ldots\ldots\ldots\ldots\ldots (32b)$$

For the hydrostatic curve of the normal component, we introduce the relation

$$f_{Nh}(\varepsilon_N) = \sigma_N = \left[\frac{C_N^0}{\left(\frac{\varepsilon_N}{\varepsilon_a} \right)^{p_H} + 1} + \frac{C_N^f}{\left(\frac{\varepsilon_N}{\varepsilon_b} \right)^{-q_H} + 1} \right] \varepsilon_N \quad \ldots\ldots\ldots\ldots\ldots\ldots (33)$$

in which C_N^f = asymptotic final modulus for normal compression as shown in Fig. 3(*b*); ε_a and ε_b = strain values that characterize the shape of the curve; and p_H (≤ 1) and q_H (> -1) = exponents that also change the shape. With this equation, we have six parameters to be fixed. Eq. (33) can control the final tangent stiffness of the hydrostatic curve; the equation of the previous model with five parameters cannot.

For the plastic curve of the normal component, the first part of the hydrostatic curve with $p_H = 1$ is adopted, for the sake of simplicity

$$f_{Np}(\varepsilon_N) = \sigma_N = \frac{C_N^0}{\left(\frac{\varepsilon_N}{\varepsilon_a} \right) + 1} \varepsilon_N \quad \ldots\ldots\ldots\ldots\ldots\ldots\ldots\ldots\ldots\ldots\ldots\ldots (34)$$

For unloading and reloading, the initial moduli of the normal component, C_N^0, are used as the linear unload-reload stiffnesses C_{Nh}^{ur0} and C_{Np}^{ur0} for the case of hydrostatic and plastic responses and also in the prepeak region of the tensile or compressive softening response. On the other hand, for the case of tensile or compressive softening after the peak stress, the following damage evolution is considered for linear unload-reload stiffness C_{Ns}^{ur0}.

For $0 \le \varepsilon_N \le \varepsilon_{NT}^0$ (prepeak tension) and $0 \ge \varepsilon_N \ge \varepsilon_{NC}^0$ (prepeak compression)

$$C_{Ns}^{ur0} = C_N^0 \quad \text{..... (35a)}$$

For $\varepsilon_N > \varepsilon_{NT}^0$ (postpeak tension)

$$C_{Ns}^{ur0} = \alpha_{NT} C_N^0 + (1 - \alpha_{NT}) \frac{\sigma_{NT}^u}{\varepsilon_{NT}^u - \xi_{NT}} \quad \text{with } \xi_{NT} = \varepsilon_{NT}^0 - \frac{\sigma_{NT}^0}{C_N^0} \quad \text{..... (35b)}$$

For $\varepsilon_N < \varepsilon_{NC}^0$ (postpeak compression)

$$C_{Ns}^{ur0} = \alpha_{NC} C_N^0 + (1 - \alpha_{NC}) \frac{\sigma_{NC}^u}{\sigma_{NC}^u - \xi_{NC}} \quad \text{with } \xi_{NC} = \varepsilon_{NC}^0 - \frac{\sigma_{NC}^0}{C_N^0} \quad \text{..... (35c)}$$

in which α_{NT}, α_{NC} = weight constants, which describe the proportions of progressive damage in tension and compression softenings; σ_{NT}^u and σ_{NC}^u = stresses at the start of unloading for tension and compression softening; ε_{NT}^u and ε_{NC}^u = strains at the start of unloading for tension and compression softening; ξ_{NT} and ξ_{NC} = plastic residual strains after complete unloading from the peak stress to zero stress. Thus, with parameter C_{Ns}^{ur0} we can control the elastoplastic-fracturing behavior for the case of softening in normal microplane component.

MICROCONSTITUTIVE LAW FOR SHEAR COMPONENTS

We know that shear behavior usually depends on the compressive stress normal to the shear plane. We will take this dependence into account in the constitutive law for the shear component on the microplane according to hypothesis IV. In the previous microplane model, this effect was modeled through the confining stress $\sigma_c = \sigma_{ii}/3$, which had the advantage that σ_{ii} is the same for all the microplanes. However, a frictional effect such as this would be better considered individually on each microplane since the shear response on each microplane is independent and the magnitudes of normal stress on various microplanes are different. Therefore, in this study it is assumed that the peak shear stress value on each microplane depends on the resolved normal component of the macroscopic stress tensor σ_{ij} on the same microplane individually. The resolved normal component S_N of the macroscopic stress tensor σ_{ij} on a microplane whose direction cosines are n_i is

$$S_N = n_j \sigma_j^n = n_j n_k \sigma_{jk} \quad \text{..... (36)}$$

The virgin loading curve of K-shear component and M-shear component must be specified as identical since they differ only in the chosen directions within the microplane. We use for shear the same form of strain-softening equation as for the normal component [Fig. 3(*a*)].

For $0 \le |\varepsilon_T| \le |\varepsilon_T^0|$ (prepeak)

$$\sigma_T = \tau^0 \left[1 - \left(1 - \frac{\varepsilon_T}{\varepsilon_T^0} \right)^{C_T^0 \varepsilon_T^0 / \tau^0} \right] \quad \text{with } \varepsilon_T^0 = \frac{\tau^0}{\zeta_T C_T^0} \quad \text{..... (37a)}$$

For $|\varepsilon_T^0| < |\varepsilon_T|$ (postpeak)

$$\sigma_T = \tau^0 \exp \left[- \left(\frac{\varepsilon_T - \varepsilon_T^0}{\sigma_T^s} \right)^{p_T} \right] \quad \text{with } \varepsilon_T^s = \gamma_T \varepsilon_T^0 = \frac{\gamma_T \tau^0}{\zeta_T C_T^0} \quad \text{..... (37b)}$$

in which subscript T refers to K-shear (TK) or M-shear (TM); τ^0 = peak stress, which depends on S_N; ζ_T = a parameter that controls the peak strain ε_T^0; and γ_T = a parameter that controls ε_T^s. At the strain $\varepsilon_T = \varepsilon_T^0 + \varepsilon_T^s$, the stress decreases to τ^0/e in the strain-softening region; p_T = a parameter controlling the shape of the softening curve. Unlike the normal component, (37) is applied for both tension and compression. The only difference between tension and compression is the sign of the peak stress τ^0; i.e., $\tau^0 > 0$ in tension and $\tau^0 < 0$ in compression.

The concept of shear frictional coefficient μ is utilized to model the dependence of shear peak stress τ^0 on S_N.

For tension of shear

$$\tau^0 = +\sigma_T^0 - \mu S_N \quad \text{when } S_N < 0 \quad \text{..... (38a)}$$

$$\tau^0 = +\sigma_T^0 \quad \text{when } S_N \ge 0 \quad \text{..... (38b)}$$

For compression of shear

$$\tau^0 = -\sigma_T^0 + \mu S_N \quad \text{when } S_N < 0 \quad \text{..... (38c)}$$

$$\tau^0 = -\sigma_T^0 \quad \text{when } S_N \ge 0 \quad \text{..... (38d)}$$

in which σ_T^0 = peak shear stress at zero normal stress. Thus, our stress-strain curve for shear has five parameters, σ_T^0, ζ_T, γ_T, p_T, and μ.

For straight-line unloading and reloading, the initial modulus of the shear component, C_T^0, is used as the linear unload-reload stiffness C_T^{ur0} in the case of the prepeak region. On the other hand, after the peak stress, the following damage evolution is considered for the linear unload-reload stiffness C_T^{ur0} for straight-line response.

For $0 \le |\varepsilon_T| \le |\varepsilon_T^0|$ (prepeak)

$$C_T^{ur0} = C_T^0 \quad \text{..... (39a)}$$

For $|\varepsilon_T| > |\varepsilon_T^0|$ (postpeak)

$$C_T^{ur0} = \alpha_T C_T^0 + (1 - \alpha_T) \frac{\sigma_T^u}{\varepsilon_T^u - \xi_T} \quad \text{with } \xi_T = \varepsilon_T^0 - \frac{\tau^0}{C_T^0} \quad \text{..... (39b)}$$

in which α_T = a weight constant that describes progressive damage for shear softening; σ_T^u, ε_T^u = stress and strain at the start of unloading; and ξ_T = plastic residual strain after complete unloading from the peak stress to zero stress. Thus, C_T^{ur0} models the elastoplastic-fracturing microconstitutive law for the softening in shear.

LOADING, UNLOADING AND RELOADING IN MICROCONSTITUTIVE RELATIONS

Macroscopic stress-strain relations for cyclic loading require proper loading-unloading-reloading criteria for each microplane component. Since our

microplane model is based on a kinematic constraint and the response on each microplane can be described only (or mainly) by microstrain components, it seems preferable to express the loading criteria in terms of microstrains only. Let each microstrain ε_N, ε_{TK}, ε_{TM} and microstress component σ_N, σ_{TK}, σ_{TM} be defined as ε and σ, for the sake of simplicity. The following loading-unloading-reloading criteria are used for all the components.

Loading

$$\text{when } \sigma_r > 0, \quad \Delta\varepsilon_{r+1} > 0, \quad \varepsilon_{r+1} \geq \varepsilon_{\max} \quad \ldots\ldots (40a)$$

$$\text{when } \sigma_r < 0, \quad \Delta\varepsilon_{r+1} < 0, \quad \varepsilon_{r+1} \leq \varepsilon_{\min} \quad \ldots\ldots (40b)$$

Unloading

$$\text{when } \sigma_r > 0, \quad \Delta\varepsilon_{r+1} < 0, \quad \varepsilon_{r+1} < \varepsilon_{\max} \quad \ldots\ldots (40c)$$

$$\text{when } \sigma_r < 0, \quad \Delta\varepsilon_{r+1} > 0, \quad \varepsilon_{r+1} > \varepsilon_{\min} \quad \ldots\ldots (40d)$$

Reloading

$$\text{when } \sigma_r > 0, \quad \Delta\varepsilon_{r+1} > 0, \quad \varepsilon_{r+1} < \varepsilon_{\max} \quad \ldots\ldots (40e)$$

$$\text{when } \sigma_r < 0, \quad \Delta\varepsilon_{r+1} < 0, \quad \varepsilon_{r+1} > \varepsilon_{\min} \quad \ldots\ldots (40f)$$

in which σ_r = microstress of each component at the end of the previous load step; ε_{r+1} = microstrain of each component at the present load step; $\Delta\varepsilon_{r+1} = \varepsilon_{r+1} - \varepsilon_r$ = incremental microstrain of each component; and $\varepsilon_{\max}$ and $\varepsilon_{\min}$ = maximum and minimum microstrains in the history.

The loading-unloading-reloading criteria in (40) with linear unload-reload stiffnesses C_N^{ur0} [(30) and (35)] and C_T^{ur0} [(39)] can be used in order to describe the cyclic behavior of each component. However, numerical simulations with C_N^{ur0} and C_T^{ur0} revealed that the hysteresis loops are too narrow. Wider hysteresis loops on the microplane are necessary to obtain proper hysteresis on the macrolevel. The reason is that hysteresis loops govern energy dissipation and the basic hypothesis of the microplane model is energy equivalence between the macro- and microlevels. Nonlinear unloading-reloading hysteresis rules with back-stress and objective-stress are developed for this purpose. The hysteresis rules are applied to the case of unloading or reloading in the strain-softening regions. The microplane back-stress σ_b is defined as

$$\sigma_{b,r+1} = \sigma_r \quad \text{when } \Delta\varepsilon_r \Delta\varepsilon_{r+1} < 0 \quad \ldots\ldots (41a)$$

$$\sigma_{b,r+1} = \sigma_{b,r} \quad \text{when } \Delta\varepsilon_r \Delta\varepsilon_{r+1} \geq 0 \quad \ldots\ldots (41b)$$

in which subscripts r and $r + 1$ refer to the previous and current numerical steps. The microplane objective-stress σ_{ob} is defined as

$$\sigma_{ob} = 0 \quad \text{when unloading} \quad \ldots\ldots (42a)$$

$$\sigma_{ob} = \sigma^u \quad \text{when reloading} \quad \ldots\ldots (42b)$$

in which σ^u = stress at the start of unloading from the virgin loading curve; σ_b and σ_{ob} are set when the microplane is unloading or reloading. We introduce the following unloading-reloading function $F^{ur}(\sigma)$ in terms of microstress σ on the unloading or reloading branch:

$$F^{ur}(\sigma) = \left| \frac{\sigma_b - \sigma}{\sigma_{ob} - \sigma_b} \right| \quad \ldots\ldots (43)$$

This function is nondimensional and its values vary from 0 to 1. The unloading tangent stiffness $C^u(\sigma)$ and the reloading tangent stiffness $C^r(\sigma)$ are (see Fig. 4)

$$C^u(\sigma) = [(U_{\min} - U_{\max})F^{ur}(\sigma) + U_{\max}]C^{ur0} \quad \ldots\ldots (44a)$$

$$C^r(\sigma) = [(R_{\min} - R_{\max})F^{ur}(\sigma) + R_{\max}]C^{ur0} \quad \ldots\ldots (44b)$$

in which $U_{\min}$ and $U_{\max}$ = nondimensional ratios determining the minimum and maximum unloading tangent stiffnesses $C^u_{\min}$ and $C^u_{\max}$ (i.e., $C^u_{\min} = U_{\min}C^{ur0}$ and $C^u_{\max} = U_{\max}C^{ur0}$; $R_{\min}$ and $R_{\max}$ = nondimensional ratios determining the minimum and maximum reloading tangent stiffnesses $C^r_{\min}$ and $C^r_{\max}$ (i.e., $C^r_{\min} = R_{\min}C^{ur0}$ and $C^r_{\max} = R_{\max}C^{ur0}$). Using the foregoing hysteresis rules, one can get hysteresis loops such as that depicted in Fig. 4(*a*).

CYCLIC LOADING RULES FOR MICROCONSTITUTIVE RELATIONS

The foregoing rules apply separately to the tension and compression regions of each microplane component. The borderline between the tension and compression regions is given by zero microplane stress. To establish a complete cyclic loading model for the microplane, the foregoing rule must be extended to the entire range of tensile and compressive microplane

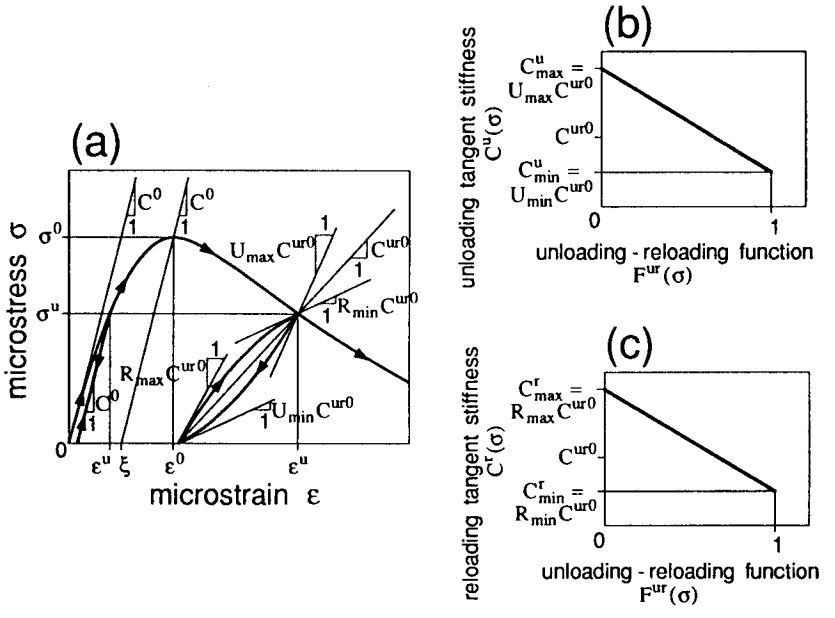

FIG. 4. (*a*) Unloadings and Reloadings from and to Points on Virgin Microstress-Strain Curve; (*b*) Unloading Tangent Stiffness $C^u(\sigma)$; (*c*) Reloading Tangent Stiffness $C^r(\sigma)$

stresses. The basic idea to do this is as follows: (1) The virgin stress-strain curves for both tension and compression are unique regardless of the number of cycles or the strain history; (2) the transition between the tension and compression regions involves horizontal plateaus; and (3) the virgin stress-strain curves can be horizontally shifted along the strain axes to the starting point of unloading or reloading. Many possible cases of the cyclic rule based on this basic idea were tried numerically and compared to the uniaxial compressive and tensile tests from the literature.

The cyclic rule for the normal component which was determined in this way is illustrated by the idealized (partially exaggerated) stress-strain curves in Fig. 5(*a*) (softening curve $f_N(\varepsilon_N)$ is used for compression). With the cyclic rule for the normal component, the origin of the compression stress-strain curve is fixed; however, the origin of the tension curve is shifted as shown. In the example of Fig. 5(*a*), the first cycle enters tensile softening, and then reverts to compression. Before going into compressive stress, there is a plateau, which corresponds to closing of microcracks. The compression region begins always at the origin (zero strain); however, the origin of tension is shifted every time when unloading from the compression region crosses the strain axis.

The cyclic rule for the shear component is shown by the idealized stress-strain curves in Fig. 5(*b*). The origins of the stress-strain curves for both tension and compression regions are fixed. In the example shown, the strain cycles are similar to those used in the previous example of normal component; however, the stress responses are very different. After the unloading curves reach the strain axis, there are always plateaus of zero stress. This assumption is needed to model experimental observations showing that for large deformations almost no stress change occurs in crack shear (aggregate interlock) tests with stress reversals. Such behavior is due to free play between asperities or between the faces of opened cracks, which need to come into contact before the stress can reverse its sign.

NONLOCAL MICROPLANE MODEL

The microplane model described so far deals only with the point properties of the macroscopic continuum approximating the average response of the heterogeneous material, under macroscopically uniform strain. This is insufficient for describing the localization phenomena and size effects. To this end, as is by now well established, one must introduce some type of a nonlocal concept.

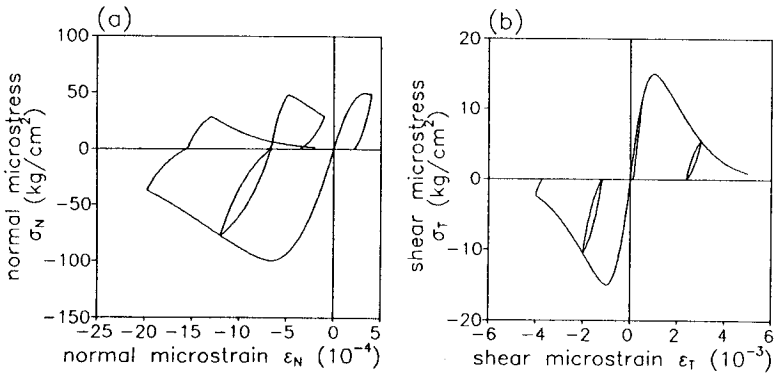

FIG. 5. (*a*) Cyclic Rule for Normal Component; (*b*) Cyclic Rule for Shear Component

In the original (imbricate) nonlocal theory (Bažant et al. 1984) the total strain was assumed to be nonlocal. But this has the disadvantage that the differential equilibrium equations and the boundary conditions are not the same as those of the local continuum theory. More recently (Pijaudier-Cabot and Bažant 1987; Bažant and Pijaudier-Cabot 1988; Bažant and Lin 1988) it has been shown that the nonlocal aspects of strain-softening can be captured while preserving the same forms of the equilibrium equations and the boundary conditions as those of the local continuum theory. In the new nonlocal damage theory, only the variables associated with strain softening are nonlocal while all the other variables, particularly the elastic strain, are local. This new nonlocal concept, which was combined with the microplane model for time-independent monotonic response of concrete in Bažant and Ožbolt (1990), is adopted in this study.

To render the microplane model nonlocal, we replace the local values of microplane stiffnesses C_N, C_{TK}, C_{TM} [(9)] and inelastic microstresses $d\sigma'_N$, $d\sigma''_{TK}$, $d\sigma''_{TM}$ [(10)] with the nonlocal values $\bar{C}_N$, $\bar{C}_{TK}$, and $\bar{C}_{TM}$ and $d\bar{\sigma}''_N$, $d\bar{\sigma}''_{TK}$, $d\bar{\sigma}''_{TM}$ (the overbars mean "nonlocal"). These nonlocal values are calculated on the basis of the nonlocal microstrains $\bar{\varepsilon}_N$, $\bar{\varepsilon}_{TK}$, $\bar{\varepsilon}_{TM}$, which represent the resolved components of the nonlocal macroscopic strain tensor $\bar{\varepsilon}_{ij}$. Thus, one always needs both local and nonlocal variables and must calculate both responses for each component on each microplane. When a microplane is loading (hardening or softening), we use the nonlocal values in (9) and (10), and when a microplane is unloading or reloading, we use the local values. The nonlocal macroscopic strain tensor $\bar{\varepsilon}_{ij}$ is calculated as

$$\bar{\varepsilon}_{ij}(\mathbf{x}) = \frac{1}{V_r(\mathbf{x})}\int_V \alpha(\mathbf{s}-\mathbf{x})\varepsilon_{ij}(\mathbf{s})\,dV = \int_V \alpha'(\mathbf{x},\mathbf{s})\varepsilon_{ij}(\mathbf{s})\,dV \quad \ldots\ldots\ldots (45)$$

in which

$$V_r(\mathbf{x}) = \int_V \alpha(\mathbf{s}-\mathbf{x})\,dV \quad \ldots\ldots\ldots (46a)$$

$$\alpha'(\mathbf{x},\mathbf{s}) = \frac{\alpha(\mathbf{s}-\mathbf{x})}{V_r(\mathbf{x})} \quad \ldots\ldots\ldots (46b)$$

$\mathbf{x}$ and $\mathbf{s}$ = coordinate vectors; $\alpha(\mathbf{x})$ = weight function, which is treated as a material property; V = volume of the entire structure; $V_r(\mathbf{x})$ has approximately but not exactly the same meaning as the representative volume in the statistical theory of heterogeneous materials.

Initially the weight function $\alpha(\mathbf{x})$ was assumed as the normal (Gaussian) distribution function. Recently Bažant proposed to use a computationally more efficient quartic bell-shaped function, which vanishes for distances greater than $r_1 = kl$ (Fig. 6)

$$\text{for } \lambda \le 1:\ \alpha(\mathbf{x}) = (1-\lambda^2)^2; \qquad \text{for } \lambda > 1:\ \alpha(\mathbf{x}) = 0 \quad \ldots\ldots\ldots (47)$$

in which $\lambda = r/r_1 = r/kl$ and for the one-dimensional case

$$r = |x_1|; \qquad k = \frac{15}{16} \quad \ldots\ldots\ldots (48a)$$

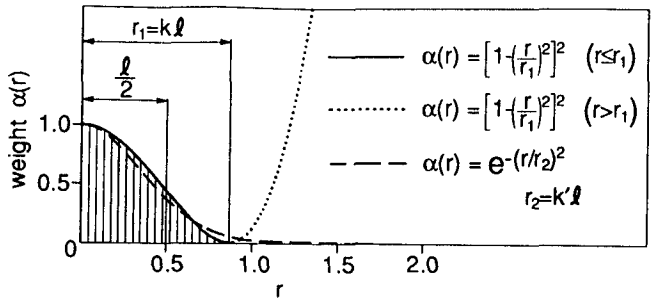

FIG. 6. Weight Functions for Nonlocal Averaging

For two-dimensional case

$$r = \sqrt{x_1^2 + x_2^2}; \qquad k = \frac{\sqrt{3}}{2} \qquad \text{(48}b\text{)}$$

For three-dimensional case

$$r = \sqrt{x_1^2 + x_2^2 + x_3^2}; \qquad k = \left(\frac{35}{64}\right)^{1/3} \qquad \text{(48}c\text{)}$$

where x_i = Cartesian coordinates; k = constants determined from the condition that the volume under the function $\alpha(\mathbf{x})$ should be equal to the volume under a function $\bar{\alpha}(\mathbf{x})$ that is uniform, $\bar{\alpha}(\mathbf{x}) = 1$ for $r \leq l/2$, and $\bar{\alpha}(\mathbf{x}) = 0$ for $r > l/2$. Here l is the characteristic length of nonlocal continuum (which gives the size of the representative volume).

NUMERICAL ALGORITHM IN FINITE-ELEMENT ANALYSIS

The present nonlocal microplane model has been introduced in a usual nonlinear finite-element program using initial stiffness method. One reason why the initial stiffness method is used is the nonsymmetry of the structural stiffness matrix, which is caused by treating only the inelasticity as nonlocal. Another reason is numerical convergence in the softening regime of the structure. Although the initial stiffness method sometimes gives slow convergence, it always converges and leads to stable iterations when the stress and strain increments due to iterations are accumulated.

In the first iteration of the first load step, the total elastic structural stiffness matrix $\mathbf{K}$ is assembled using the specified Young's modulus and Poisson's ratio of the material. In each load step, the following numerical algorithm is employed.

1. At the beginning of each iteraction, $\mathbf{K}$ is used to estimate a trial structural incremental displacement vector $\Delta\mathbf{u}$ by solving the equation $\Delta\mathbf{u} = \mathbf{K}^{-1}\Delta\mathbf{f}$, where $\Delta\mathbf{f}$ is the nodal force increment due to prescribed force and displacement at the present load step or the residual nodal force from the previous iteration. Then one calculates the incremental local macroscopic strains $\Delta\varepsilon_{ij}$ for all the integration points of all finite elements, and also the incremental nonlocal macroscopic strains $\Delta\bar{\varepsilon}_{ij}$ from (45) and (46).
2. The incremental local microstrains $\Delta\varepsilon_N$, $\Delta\varepsilon_{TK}$, and $\Delta\varepsilon_{TM}$ are calculated for each microplane at each integration point of each finite element using (1) and (3) with $\Delta\varepsilon_{ij}$. The incremental nonlocal microstrains $\Delta\bar{\varepsilon}_N$, $\Delta\bar{\varepsilon}_{TK}$, and $\Delta\bar{\varepsilon}_{TM}$ are also evaluated from $\Delta\bar{\varepsilon}_{ij}$. Then, for normal, K-shear, and M-shear components of both local and nonlocal strains on each microplane, loading, unloading, or reloading is judged using (40). Depending on the loading-unloading-reloading condition, the local and nonlocal values of the microstiffnesses C_N, C_{TK}, C_{TM}, $\bar{C}_N$, $\bar{C}_{TK}$, and $\bar{C}_{TM}$ and the local and nonlocal inelastic microstresses $d\sigma''_N$, $d\sigma''_{TK}$, $d\sigma''_{TM}$, $d\bar{\sigma}''_N$, $d\bar{\sigma}''_{TK}$, and $d\bar{\sigma}''_{TM}$ are calculated based on the aforementioned microconstitutive models. If there is hardening or softening (virgin loading) on a microplane we use the nonlocal microstiffnesses and inelastic microstresses; on the other hand, if unloading or reloading occurs on a microplane, the local values are used to calculate macroscopic incremental stiffness C_{ijrs} [(9)] and macroscopic inelastic stress increment $d\sigma''_{ij}$ [(10)] for the integration point of the finite element. Then the macroscopic total stress increment $d\sigma_{ij}$ [(18)] and the macroscopic total stress σ_{ij} are calculated.
3. Based on the calculated total stresses at each integration point in each finite element, the total equivalent nodal forces $\mathbf{f}^{EQ}$ are evaluated and assembled for the whole structure. The residual nodal forces $\mathbf{f}^R$ are calculated as $\mathbf{f}^R = \mathbf{f} - \mathbf{f}^{EQ}$, in which $\mathbf{f}$ is the total nodal force due to the prescribed force and displacement at the present load step, or the residual nodal force of the previous iteration.
4. The norm ratio ω of the residual nodal forces, defined as $\omega = [\Sigma\,(\mathbf{f}^R)^2/\Sigma\,(\mathbf{f})^2]^{1/2}$, is calculated to judge convergence of the iterations. In this study, if $\omega \leq 0.01$, the iteration process is judged to have converged, and the calculation advances to the next load step. If $\omega > 0.01$, one returns to step 1 and starts the next iteration.

To implement the step-by-step calculation, a number of characteristic microstrain and microstress values for each microplane need to be stored in the computer memory. Their number is 43 ($= 15 + 2 \times 14$) per microplane (Table 1). Since in this study the Bažant and Oh's (1986) integration

TABLE 1. Characteristic Values for State of Each Microplane to Be Stored in Memory

Value		Normal		Shear K and M	
(1)	(2)	Tension (3)	Compression (4)	Tension (5)	Compression (6)
Strain in previous iteration	ε_r	○	○	○	○
Maximum strain	ε_{max}	○	—	○	—
Minimum strain	ε_{min}	—	○	—	○
Strain at back-stress	ε_b	○	○	○	○
Strain at zero stress after complete unloading	ε_p	○	○	○	○
Strain at origin of curve	ε_z	○	—	—	—
Stress in previous iteration	σ_r	○	○	○	○
Stress at start of unloading	σ^u	○	○	○	○
Back-stress	σ_b	○	○	○	○
Linear unload-reload stiffness	C^{ur0}	○	○	○	○

Note: ○ means necessary to be stored in memory.

formula with 21 points on a hemisphere is used [Fig. 1(*d*)], and since we have both local and nonlocal components, we need to store 1,806 ($=2 \times 21 \times 43$) values for each integration point of each finite element.

CONCLUSION

The present improved and extended formulation of the microplane model for concrete bears considerable promise with regard to numerical finite-element analysis of concrete structures. [Application to the analysis of test data is done in part II (Hasegawa and Bažant 1993); in which detailed conclusions are to be found.]

ACKNOWLEDGMENT

The present results have been obtained under a joint research program between Shimizu Corporation, Tokyo, and Northwestern University. The first author wishes to thank Shimizu Corporation for giving him the opportunity to conduct this research at Northwestern University.

APPENDIX. REFERENCES

Bažant, Z. P. (1971). "Numerically stable algorithm with increasing time steps for integral-type aging creep." *Proc., 1st Int. Conf. on Struct. Mech. in Reactor Technol.*, T. A. Jaeger, ed., West Berlin, Germany, 4, Part H, 119–126.

Bažant, Z. P. (1984). "Microplane model for strain-controlled inelastic behavior." *Mechanics of engineering materials*, C. S. Desai and R. H. Gallagher, eds., John Wiley and Sons, New York, N.Y., 45–59.

Bažant, Z. P. (1988). "Improvements of microplane model." *Int. Res. Notes*, Northwestern University, Evanston, Ill.

Bažant, Z. P., Belytschko, T. B., and Chang, T.-P. (1984). "Continuum theory for strain-softening." *J. Engrg. Mech.*, ASCE, 110(12), 1666–1692.

Bažant, Z. P., and Chern, J.-C. (1985). "Strain softening with creep and exponential algorithm." *J. Engrg. Mech.*, ASCE, 111(3), 391–415.

Bažant, Z. P., and Lin, F.-B. (1988). "Nonlocal smeared cracking model for concrete fracture." *J. Struct. Engrg.*, ASCE, 114(11), 2493–2510.

Bažant, Z. P., and Oh, B. H. (1985). "Microplane model for progressive fracture of concrete and rock." *J. Engrg. Mech.*, ASCE, 111(4), 559–582.

Bažant, Z. P., and Oh, B. H. (1986). "Efficient numerical integration on the surface of a sphere." *Zeitschrift für Angewandte Mathematik und Mechanik*, Leipzig, Germany, 66(1), 37–49.

Bažant, Z. P., and Ožbolt, J. (1990). "Nonlocal microplane model for fracture, damage, and size effect in structures." *J. Engrg. Mech.*, ASCE, 116(11), 2485–2505.

Bažant, Z. P., and Pijaudier-Cabot, G. (1988). "Nonlocal continuum damage, localization instability and convergence." *J. Appl. Mech.*, 55(2), 287–293.

Bažant, Z. P., and Prat, P. C. (1988a). "Microplane model for brittle-plastic material: I. Theory." *J. Engrg. Mech.*, ASCE, 114(10), 1672–1680.

Bažant, Z. P., and Prat, P. C. (1988b). "Microplane model for brittle-plastic material: II. Verification." *J. Engrg. Mech.*, ASCE, 114(10), 1689–1702.

Carol, I., Bažant, Z. P., and Prat, P. C. (1992). "New explicit microplane model for concrete: Theoretical aspects and numerical implementation." *Int. J. Solids and Struct.*, 29(9), 1173–1191.

Hasegawa, T., and Bažant, Z. P. (1991). "Nonlocal microplane model with rate effect for concrete." *Struct. Engrg. Rep., 91-9/919*, Department of Civil Engineering, Northwestern University, Evanston, Ill.

Hasegawa, T., and Bažant, Z. P. (1993). "Nonlocal microplane concrete model with rate effect and load cycles. II: Application and verification." *J. Mat. In Civ. Engrg.*, ASCE, 5(3), 372–393.

Ožbolt, J., and Bažant, Z. P. (1991). "Cyclic microplane model for concrete." *Proc. Int. RILEM/ESIS Conf. on fracture processes in brittle disordered materials: concrete, rock, ceramics*, Chapman & Hall, London, England, 639–650.

Pijaudier-Cabot, G., and Bažant, Z. P. (1987). "Nonlocal damage theory." *J. Engrg. Mech.*, ASCE, 113(10), 1512–1533.

Taylor, G. I. (1938). "Plastic strain in metals." *J. Inst. Metals*, 62, 307–324.

NONLOCAL MICROPLANE CONCRETE MODEL WITH RATE EFFECT AND LOAD CYCLES. II: APPLICATION AND VERIFICATION

By Toshiaki Hasegawa[1] and Zdeněk P. Bažant,[2] Fellow, ASCE

ABSTRACT: This second part of the study deals with experimental verification of an improved and generalized nonlocal microplane model whose general formulation was given in the first part. First the stress-strain relations for a material point are simulated with a local version of the model, and then the representation of some basic tests is studied in finite-element analyses with the nonlocal calculation.

INTRODUCTION

Part I of this study (Hasegawa and Bažant 1993) presented various improvements and extensions of the microplane model for concrete. The purpose of this second part is to demonstrate the capability to simulate the pertinent test data. All definitions and notations from part I are retained.

The postpeak response of specimens with strain-softening damage or fracture must be suspected to involve strain localization and size effect, and cannot be interpreted as if the specimens were in a uniform state. This means that the numerical results we get with one finite element using a local version of the microplane model are insufficient to compare with the experimental results and verify the model. Subdivision of the specimens into many finite elements is needed to do that. Nevertheless, as the first check of the constitutive model, the point response, calculated with one finite element, needs to be explored and understood.

SIMULATION OF MACROSCOPIC STRESS-STRAIN RELATION FOR MATERIAL POINT

Except for the elastic constants, Young's modulus E and Poisson's ratio ν, each microplane in the present model is characterized by three groups of material parameters: The first group involves the material parameters for the virgin stress-strain curves, i.e. σ_{NT}^0, ζ_{NT}, γ_{NT}, and p_{NT} for (31) of part I; σ_{NC}^0, ζ_{NC}, γ_{NC}, and p_{NC} for (32) of part I; σ_T^0, ζ_T, γ_T, p_T, and μ for (37) and (38) of part I; C_N^f, ε_a, ε_b, p_H, and q_H for (33) and (34) of part I; and ε_{LD}^t, ε_{LD}^v, and m for (27) of part I. The second group involves the material parameters for unloading-reloading, i.e. α_{NT} and α_{NC} for (35) of part I; α_T for (39) of part I; and $U_{\max}$, $U_{\min}$, $R_{\max}$, and $R_{\min}$ for (44) of part I. The third group involves the relaxation times ρ in (12) of part I. For $U_{\max}$, $U_{\min}$, $R_{\max}$, $R_{\min}$ and ρ we have separate values for normal tension, normal compression, and shear. Altogether, there are 39 material parameters. However, according to the data-fitting experience it appears that one does not have to specify the individual values for α_{NT}, α_{NC}, and α_T as well as those for $U_{\max}$, $U_{\min}$, $R_{\max}$, and $R_{\min}$ in normal tension, normal compression, and shear. Also, it appears that one can set $U_{\max} = R_{\max}$ and $U_{\min} = R_{\min}$ because, if $U_{\max} \neq R_{\max}$ or $U_{\min} \neq R_{\min}$, the shapes of the hysteresis loops are sometimes unacceptable. It means that we can reduce the number of independent microplane material parameters to 27.

By fitting cyclic uniaxial compressive and tensile test data for concrete, the following values characterizing the unloading-reloading rule were found to work:

$$U_{\max} = R_{\max} = 2.0 \quad \ldots\ldots (1a)$$

$$U_{\min} = R_{\min} = 0.5 \quad \ldots\ldots (1b)$$

$$\alpha_{NT} = \alpha_{NC} = \alpha_T = 0.2 \quad \ldots\ldots (1c)$$

In the case of normal hydrostatic response, the hysteresis loops of a microplane should be very narrow because little damage is done to the material; in the case of normal compressive softening response, the hysteresis loops should be wide. However, no hysteresis is assumed for normal compressions including softening, for the sake of simplicity.

Since under hydrostatic condition there is no shear on the microplanes, the material parameters C_N^f, ε_a, ε_b, p_H, and q_H for the hydrostatic curve [(33) of part I] can be determined independently of all the others, simply by direct fitting of the experimental data for hydrostatic compression of concrete. Such a fitting of the test data of Green and Swanson (1973) is shown in Fig. 1(*a*), and the material parameters identified are $C_N^f = C_N^0$; $\varepsilon_a = -0.0013$; $\varepsilon_b = -0.17$; and $p_H = q_H = 1.0$. Although there exist only limited hydrostatic compression test data for concrete, they show that we may assume the asymptotic final modulus (slope) for the hydrostatic curve to be the same as the initial modulus, i.e., $C_N^f = C_N^0$. For most individual data sets of concrete, the hydrostatic response curve has not been measured, and therefore the parameters determined for the test data of Green and Swanson are used in all the present calculations.

Since in most static loading tests of concrete only one strain rate has been used, it is impossible to identify the microplane material parameters governing the rate effect, i.e. relaxation times ρ. Therefore, in the following

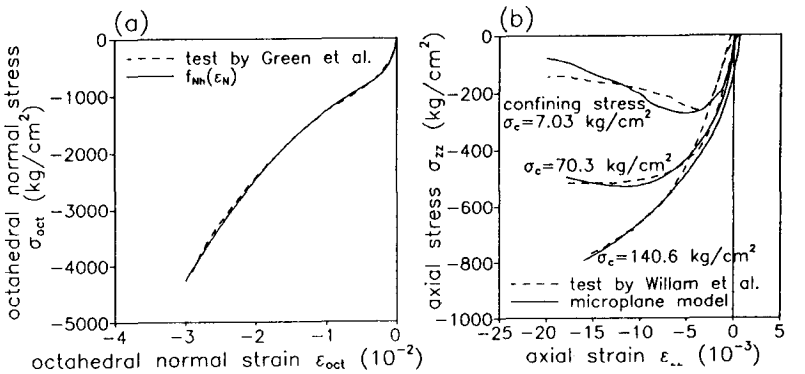

FIG. 1. (*a*) Comparison with Hydrostatic Compression Test by Green and Swanson (1973); (*b*) Comparison with Triaxial Compressive Tests by Willam et al. (1986)

[1]Struct. Res. Engr., Shimizu Corp., 3-4-17 Etchujima, Koto-ku, Tokyo 135, Japan.
[2]Walter P. Murphy Prof. of Civ. Engrg., Northwestern Univ., 2145 Sheridan Rd., Evanston, IL 60208-3109.

Note. Discussion open until January 1, 1994. Separate discussions should be submitted for the individual papers in this symposium. To extend the closing date one month, a written request must be filed with the ASCE Manager of Journals. The manuscript for this paper was submitted for review and possible publication on September 23, 1991. This paper is part of the ***Journal of Materials in Civil Engineering***, Vol. 5, No. 3, August, 1993. ©ASCE, ISSN 0899-1561/93/0003-0394/$1.00 + $.15 per page. Paper No. 2742.

calculations for the static loading tests we have to eliminate the strain rate effect by specifying infinite values of the relaxation times ρ^z. According to the numerical simulations of one microplane response with different relaxation times and strain rates, the values of the relaxation times ρ^z seem to be functions of the strain rate and the peak stress value for the monotonic curve. In the case of calculations for the typical static strain rates used in experiments, $\dot{\varepsilon} = 10^{-6}$–$10^{-5}$/s, it seems possible to consider the relaxation times $\rho^{\infty}_{NT} = \rho^{\infty}_{T} = 10^5$ s and $\rho^{\infty}_{NC} = 10^6$ or 10^7 s as infinite.

First some comparisons with the previous microplane model should be mentioned. In the previous microplane model (Bažant and Prat 1988; Bažant and Ožbolt 1990; Ožbolt and Bažant 1991; Carol et al. 1992), a good description of the response in compression softening was achieved by splitting the resolved normal microstrain component into volumetric and deviatoric components, which meant that the microplane response was indirectly affected by the lateral strain. This split made it possible to describe materials with arbitrary Poisson ratios ν, within the range $-1 \leq \nu \leq 0.5$, which is an advantage over the present model (in which an arbitrary Poisson's ratio cannot be obtained). However, the fact that the lateral strain has only an indirect effect, as a part of the volumetric strain, may be a disadvantage, detracting from conceptual clarity. Whereas the differences in the capabilities of these two related but different approaches remain to be explored deeper, we adhere here to the direct use of lateral strain, with no volumetric-deviatoric split of the normal strain.

Fig. 2 shows an example of response for the uniaxial compressive test, in which the formulations for the volumetric, deviatoric and shear components on all microplanes are combined. The material parameter values are as follows: (1) For volumetric tension $\sigma^0_{VT} = 2.45$ MPa, $\zeta_{VT} = 0.9$, γ_{VT}

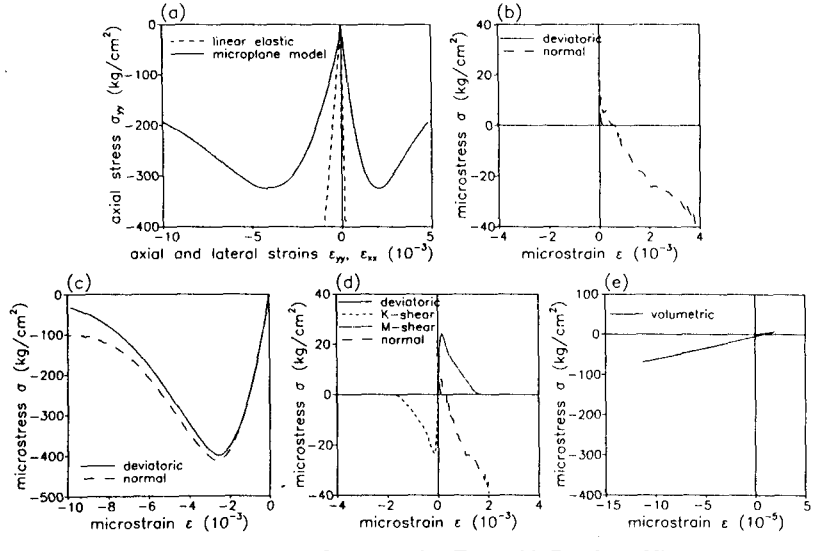

FIG. 2. Responses for Uniaxial Compressive Test with Previous Microplane Model: (a) Macroscopic Stress-Strain Response; (b) Microstress-Strain Responses at Integration Point 1; (c) Microstress-Strain Responses at Integration Point 2; (d) Microstress-Strain Responses at Integration Point 18; (e) Volumetric Response

$= 3.0$, $p_{VT} = 2.0$, $\rho_{VT} = 10^5$ s, and $\eta_0 = C^0_D/C^0_V = 1.0$; (2) for deviatoric tension $\sigma^0_{DT} = 0.49$ MPa, $\zeta_{DT} = 0.9$, $\gamma_{DT} = 3.0$, $p_{DT} = 2.0$, and $\rho_{DT} = 10^5$ s; (3) for deviatoric compression $\sigma^0_{DC} = -39.23$ MPa, $\zeta_{DC} = 0.5$, $\gamma_{DC} = 1.5$, $p_{DC} = 1.5$, and $\rho_{DC} = 10^6$ s; and (4) for shear $\sigma^0_T = 1.47$ MPa, $\zeta_T = 0.5$, $\gamma_T = 1.5$, $p_T = 1.5$, $\mu = 1.0$, and $\rho_T = 10^5$ s. The numerical integration over the spherical surface of microplane orientations was done using Bažant and Oh's (1986) formula with 21 integration points per hemisphere [Fig. 1(*d*) of part I]. (The uniaxial compression direction coincided with the direction of the unit normal vector at integration point 2.) Fig. 2(*a*) shows the macroscopic stress-strain curve and Figs. 2(*b–d*) show for integration points 1, 2, and 18 (the deviatoric response and the shear responses of the K and M directions) and the total normal response as a sum of the deviatoric and volumetric components. Fig. 2(*e*) shows the volumetric response. The microplane at integration point 2 affects mainly the axial response, while the microplane at integration point 1 affects mainly the Poisson effect and volume dilatancy. The microplane at integration point 18 has a high intensity of shear strain, while integration points 1 and 2 have no shear strains.

Since a few existing hydrostatic tension tests show that the macroscopic hydrostatic tensile strength of concrete is approximately equal to the macroscopic uniaxial tensile strength f_t, we have to choose the volumetric peak tensile stress value σ^0_{VT} equal to the macroscopic uniaxial tensile strength f_t. However, the macroscopic uniaxial tensile peak stress calculated with the microplane volumetric-deviatoric-shear formulation is then higher than the sum of the deviatoric peak tensile stress value σ^0_{DT} and the volumetric peak tensile stress σ^0_{VT}. This means that we should set σ^0_{VT} as close to f_t as possible and σ^0_{DT} as small as possible because a reasonable triaxial failure envelope in the tensile region could not otherwise be obtained. Therefore, in calculating Fig. 2, a small value of σ^0_{DT} ($=0.49$ MPa) and a larger value of σ^0_{VT} ($=2.45$ MPa) were chosen. But this goes against the assumption of the previous model that the stress-strain curves for volumetric tension and deviatoric tension are the same. The use of a small value of σ^0_{DT} causes the damage on each microplane to occur earlier, especially on the microplanes that resist lateral dilation in the case of uniaxial compression; this causes a deviation from purely elastic behavior at lower stress level. This is the reason why the response seen in Fig. 2(*a*) is far away from purely elastic behavior [dotted straight lines in Fig. 2(*a*)] already at the beginning of stressing. To avoid this, a material constant η_0 ($= C^0_D/C^0_V$), representing the ratio between the initial deviatoric and volumetric moduli, was changed for these calculations, but no better result had been available.

One interesting result is the volumetric response, which shows a volumetric dilatation to occur at the beginning and a volumetric compaction after that, as seen in Fig. 2(*e*). It is an opposite trend to that in the study of Bažant and Prat (1988), in which reasonable results were obtained showing the initial volumetric compaction and subsequent volumetric dilatation. The reason was the assumption that $\sigma^0_{DT} = \sigma^0_{VT}$ and that the stress-strain curves for deviatoric and volumetric tensions are the same. However, the assumption $\sigma^0_{DT} = \sigma^0_{VT}$ appears questionable from the viewpoint of the macroscopic triaxial strength envelope, as already mentioned.

To compare the present normal-shear formulation with the previous volumetric-deviatoric-shear formulation, Fig. 3 presents the numerical results for uniaxial compression using the present microplane model, and Table 1 gives the corresponding material parameters. Fig. 3(*a*) shows the calculated

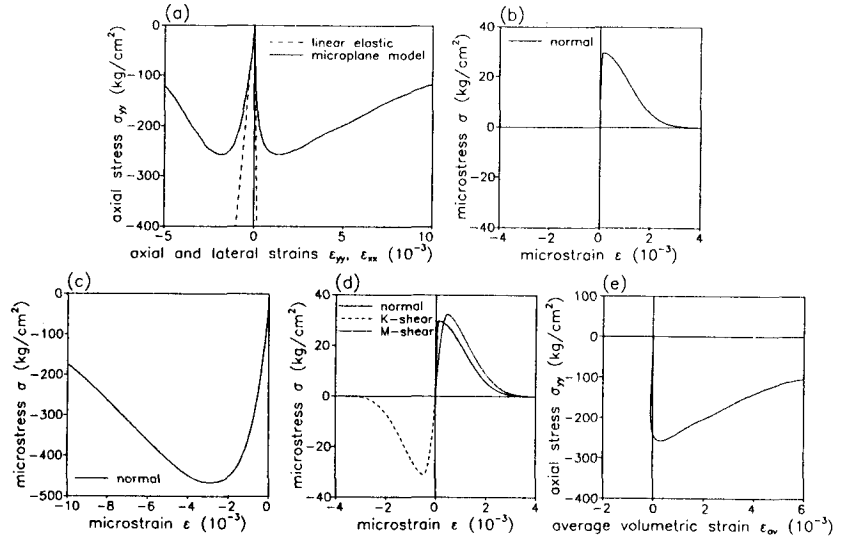

FIG. 3. Responses for Uniaxial Compressive Test with Present Microplane Model: (a) Macroscopic Stress-Strain Response; (b) Microstress-Strain Response at Integration Point 1; (c) Microstress-Strain Response at Integration Point 2; (d) Microstress-Strain Responses at Integration Point 18; (e) Macroscopic Volumetric Response

macroscopic stress-strain response. Figs. 3(*b–d*) show the normal, *K*-shear, and *M*-shear responses for integration points 1, 2, and 18 (the same as in Fig. 2). Fig. 3(*e*) shows the resulting relation between the macroscopic axial stress σ_{yy} and the macroscopic average volumetric strain ε_{av} ($\varepsilon_{av} = \varepsilon_{ii}/3$). Compared with the responses on the microplanes in the previous formulation (Fig. 2), the responses for the present formulation appear quite reasonable. The response at integraton point 1 is a progressive tensile softening behavior, which reflects axial tensile cracking in the uniaxial compressive specimen [Fig. 3(*b*)]. In the calculation, the macroscopic compressive peak is obtained when the shear responses on some microplanes (integration points 4, 5, 6, 7, 10, 11, 12, and 13) go into the softening regimes after the normal responses on the same microplanes go into softening. This appears to be a consistent picture of the micromechanism of uniaxial compressive failure, in which the uniaxial compressive specimen is weakened by axial splitting cracks. The main difference from the results with the previous formulation is the relation between the macroscopic axial stress σ_{yy} and the macroscopic average volumetric strain ε_{av}, shown in Fig. 3(*e*). In contrast to the previous formulation [Fig. 2(*e*)], the present volumetric response is consistent with the experimental fact that the volumetric compaction precedes the volumetric dilatation due to axial tensile cracking. The turning point from volumetric compaction to dilatation, which is sometimes called the critical point and occurs in experiments usually at 75–90% of uniaxial compressive strength f'_c, is here obtained at 78% of f'_c.

Fig. 1(*b*) shows the fits of the triaxial compressive test data for concrete by Willam et al. (1986), and Table 1 gives the material parameters used. These tests, which were carried out at three different confining stress levels

TABLE 1. Optimum Values of Material Parameters

Material Parameter (1)	(2)	(3)	Fig. 3 (4)	Willam et al. (1986) (5)	van Mier (1984) (6)	Karsan and Jirsa (1969) (7)	Reinhardt and Cornelissen (1984) (8)	Dilger et al. (1984) (9)
Normal tension	σ^0_{NT}	kg/cm²	30.0	26.0	65.0	26.0	21.0	45.0
	ζ_{NT}	—	0.5	0.5	0.5	0.5	0.6	0.5
	γ_{NT}	—	15.0	5.0	5.0	10.0	5.0	10.0
	p_{NT}	—	2.0	1.5	1.5	1.5	1.5	1.5
	ρ_{NT}	sec	10^5	10^5	10^5	10^5	10^5	3.0×10^2
Normal compression (softening)	σ^0_{NC}	kg/cm²	−400.0	−340.0	−640.0	−300.0	−600.0	−350.0
	ζ_{NC}	—	0.2	0.4	0.3	0.4	0.4	0.4
	γ_{NC}	—	2.0	2.0	2.0	2.0	2.0	2.0
	p_{NC}	—	1.5	1.5	1.5	1.5	1.5	1.5
	ρ_{NC}	sec	10^6	10^7	10^7	10^7	10^7	3.0×10^3
Shear	σ^0_T	kg/cm²	15.0	15.0	50.0	10.0	10.0	15.0
	ζ_T	—	0.5	0.6	0.8	0.8	0.8	0.8
	γ_T	—	3.0	2.0	1.5	6.0	1.5	4.0
	p_T	—	1.5	1.5	1.5	1.5	1.5	1.5
	μ	—	0.5	1.0	0.5	0.5	0.5	0.5
	ρ_T	sec	10^5	10^5	10^5	10^5	10^5	3.0×10^2
Lateral strain effect	ε^1_{LD}	—	0.002	0.01	0.01	0.01	0.01	0.01
	ε^2_{LD}	—	0.002	0.01	0.01	0.01	0.01	0.01
	m	—	1.0	1.0	1.0	1.0	1.0	1.0
Experimental data	f'_c	kg/cm²	—	225.0	431.0	193.0[a]	463.0[b]	237.0
	f_t	kg/cm²	—	26.0	28.0[c]	—	23.0[a]	—

[a]Peak stress in test.
[b]Cubic specimen.
[c]Concrete of a different batch with the same mix proportion.

(σ_c = 0.69, 6.90, and 13.79 MPa), show the confinement effect, i.e., the transition from the softening response at σ_c = 0.69 MPa to the plastic hardening response at σ_c = 13.79 MPa. The feature that enables the present microplane model to describe the confinement effect is the dependence of the normal response on the lateral strains and also the dependence of the peak shear microstress value on the resolved normal macroscopic stress tensor. The former dependence is included in parameter ε^l_{LD}, ε^p_{LD}, and m, and the latter dependence is included in parameter μ. The fits in Fig. 1(b) are good, which means that the present normal-shear formulation with lateral strain dependence and the resolved normal macroscopic stress tensor dependence is valid without resorting to the volumetric-deviatoric subdivision of the normal microplane strain. The other tests simulated in this study include no data with different confining stress levels, therefore in the latter calculations the parameters fitted to the test data of Willam et al. (1986), ε^l_{LD} = 0.01, ε^p_{LD} = 0.01, and m = 1.0, are used for the sake of simplicity.

Figs. 4 and 5 show the fits of the cyclic uniaxial compressive tests of concretes by van Mier (1984) and by Karsan et al. (1960), and Table 1 lists the corresponding material parameters. As before, Fig. 4(b–d) and Fig. 5(b–d) show the normal, K-shear and M-shear responses at integration points 1, 2, and 18. From these results we can see a good capability of the present model in describing macroscopic cyclic behaviors including degradation of the unloading-reloading stiffness and the shapes of the hysteresis loop, particularly the change of the loop width. The integration points 1 correspond to the lateral directions for uniaxial compression and their responses simulate axial splitting cracks. Note that even though the microplane

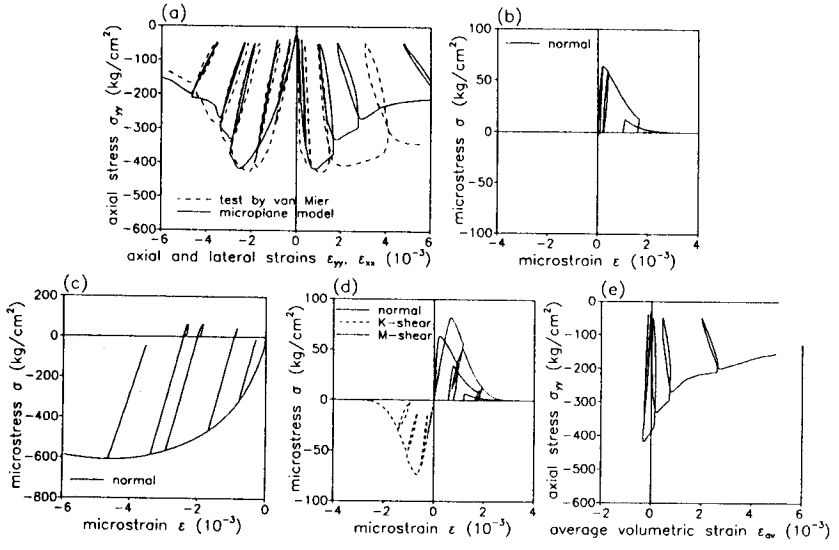

FIG. 4. Comparison with Cyclic Uniaxial Compressive Test by van Mier (1984): (*a*) Macroscopic Stress-Strain Response; (*b*) Microstress-Strain Response at Integration Point 1; (*c*) Microstress-Strain Response at Integration Point 2; (*d*) Microstress-Strain Responses at Integration Point 18; (*e*) Macroscopic Volumetric Response

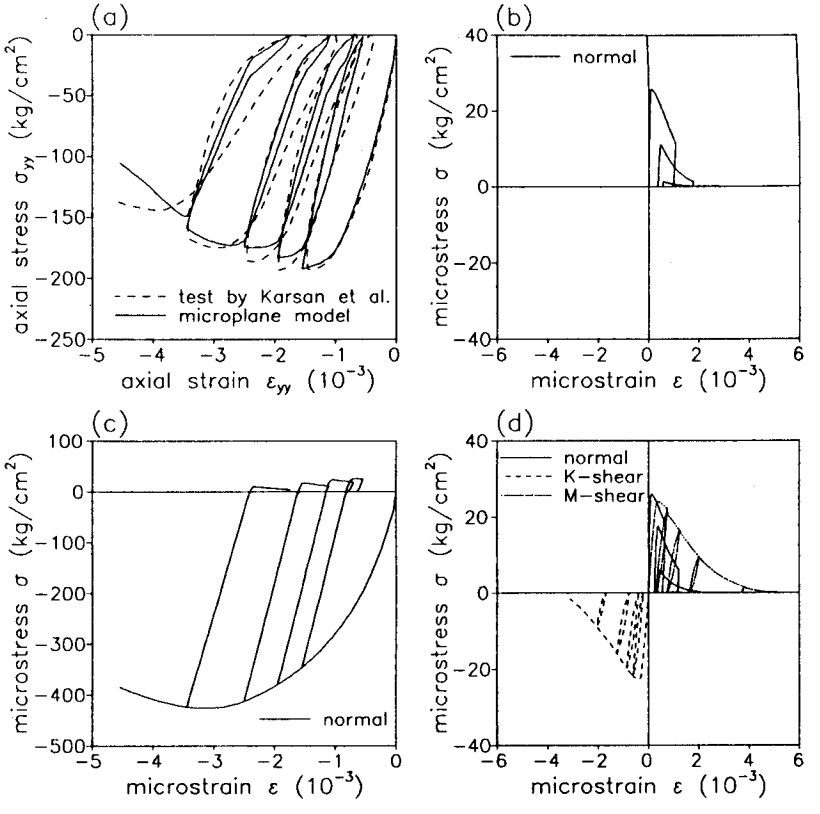

FIG. 5. Comparison with Cyclic Uniaxial Compressive Test by Karsan and Jirsa (1969): (*a*) Macroscopic Stress-Strain Response; (*b*) Microstress-Strain Response at Integration Point 1; (*c*) Microstress-Strain Response at Integration Point 2; (*d*) Microstress-Strain Responses at Integration Point 18

responses at integration points 2 corresponding to the direction of uniaxial compression have no hysteresis loops, the macroscopic responses for the same strain values as those for integration points 2 do have hysteresis loops. It means that the source of macroscopic hysteresis lies mainly in the hysteresis loops for normal tensile softening and shear softening on the microplanes.

Fig. 6 compares the calculated results with Reinhardt's (1984) cyclic uniaxial tensile tests, in which tapered cylindrical specimens were used, with saw-cut notches inducing a crack at mid length. The displacement across the notch was measured over the base length of 25 mm. The average strain over the base length was compared to the present calculations. The identified material parameters are again listed in Table 1. The calculated results agree well with these test data, especially the postpeak stiffness degradation and the linear compressive behavior.

Fig. 7(a) compares the uniaxial compressive tests data (Dilger et al. 1984) for different strain rates (-3.3×10^{-5} to -2.0×10^{-1} s^{-1}) with the calculated results using the relaxation times ρ given, along with other material parameters, in Table 1. The ρ-values have totally different orders of

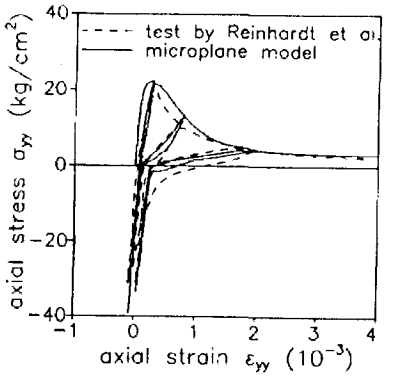

FIG. 6. Comparison with Cyclic Uniaxial Tensile Test by Reinhardt and Cornelissen (1984)

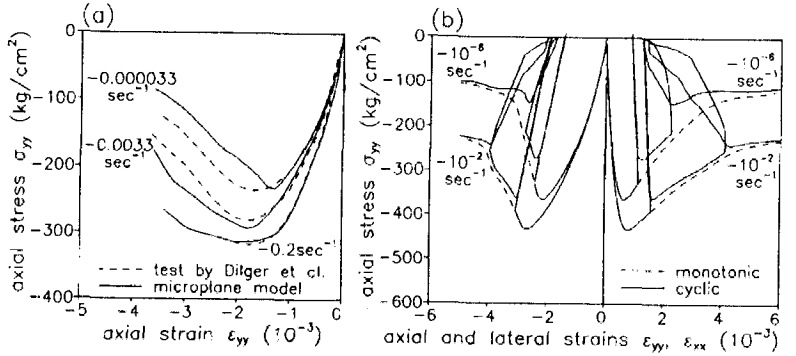

FIG. 7. (*a*) Comparison with Uniaxial Compressive Tests for Different Strain Rates by Dilger et al. (1984); (*b*) Prediction of Cyclic Responses with Different Strain Rates, Using Material Parameters Corresponding to van Mier's (1984) Test Data

magnitude than in the previous static calculations because the strains range from static to dynamic (impact). In the calculation, different values of Young's modulus E are used for different strain rates, since, otherwise, the initial prepeak response would deviate from the test results (for $\dot{\varepsilon} = 3.3 \times 10^{-5}$, -3.3×10^{-3}, and -2.0×10^{-1} s^{-1}: $E = 3.24 \times 10^4$, 3.43×10^4, and 4.22×10^4 MPa). (This could be avoided by introducing strain-rate dependence in the elastoplastic-fracturing element of the generalized Maxwell model for each microplane, but this would further complicate the model.) Although the fits are not poor, more extensive comparisons are desirable.

There are only few experimental data on the strain rate effect, especially for cyclic loading. We consider van Mier's (1984) cyclic uniaxial compression data. The relaxation times are assumed as $\rho_{NT} = \rho_T = 1.0 \times 10^4$ s; $\rho_{NC} = 1.0 \times 10^5$ s; and the monotonic and cyclic loading calculations are done for two strain rates, $\dot{\varepsilon} = -1.0 \times 10^{-6}$ and -1.0×10^{-2} s^{-1}. In each, the unloading-reloading cycles start at two postpeak stress values $0.9\sigma_{peak}$ and $0.6\sigma_{peak}$, where σ_{peak} = peak stress for monotonic loading. The results are shown in Fig. 7(*b*). The decreases of the load capacities due to cycling,

which are defined as stress differences between the monotonic and cyclic curves, get smaller as the strain rate gets larger.

One advantage of the present microplane model is that each material parameter has a clear, easily understandable, mechanical meaning. For example, σ^0 are the peak microstresses for each component, γ represent the ductilities in the postpeak range, and ζ represent the strains at peak stress, characterizing the degree of nonlinearity in the prepeak response. The values in Table 1 illuminate the choice of material parameters for the microplane model; σ^0_{NT} and σ^0_T appear to be related not only to f_t but also to f'_c; σ^0_{NT} can control the stress level for the critical point of uniaxial compressive stress-strain curve; σ^0_{NC} does not have a strong correlation with f'_c, but we might consider it to be larger than f'_c. From numerical experience, $\sigma^0_{NT} = (1.0\text{–}2.0)f_t$, $\sigma^0_{NC} \cong -1.5f'_c$, and $\sigma^0_T = (0.5\text{–}1.5)f_t$. The values of ζ_{NT} and ζ_{NC} do not have large effects on the macroscopic behavior; however, ζ_{NC} must be chosen so that the normal compressive softening curve touches inside of the normal hydrostatic curve. On the other hand, the value of ζ_T can change the macroscopic peak stress and the ductilities in uniaxial compressive test. From numerical experience, $\zeta_{NT} = 0.4\text{–}0.6$, $\zeta_{NC} = 0.3\text{–}0.5$, and $\zeta_T = 0.4\text{–}0.8$. There seems to be a tendency of large γ_{NT} and γ_T values to yield higher peak stresses and ductilities in the macroscopic responses. The value γ_{NC} seems to have a small effect on the macroscopic uniaxial compressive and tensile behaviors. The values p_{NT}, p_{NC}, and p_T change the postpeak softening curves only slightly (the ductilities depend mainly on γ). From such experience, $p_{NT} = p_{NC} = p_T = 1.5$. The larger the frictional coefficient μ of the shear component, the more prominent the confinement effect in triaxial tests. However, if μ becomes too large, the volumetric dilatation near the uniaxial peak stress disappears. From experience, $\mu = 0.5\text{–}1.0$.

With the foregoing parameters fixed as indicated, 10 material parameters remain to be identified by fitting individual monotonic test data (namely σ^0_{NT}, σ^0_{NC}, σ^0_T, ζ_{NT}, ζ_{NC}, ζ_T, γ_{NT}, γ_{NC}, γ_T, and μ) provided that the parameters of the hydrostatic curve and the lateral strain effect have already been fixed.

Note that all the test data used were obtained at fixed principal stress rotations. We cannot guarantee that if their directions rotate, some modifications of the model might not be needed. In principle, however, the microplane model should apply to rotating principal stress directons as well.

As important feature to note is that the test data were fitted under the assumption of a uniform strain state. Obviously this is generally not true for postpeak softening. Localizations likely occurred, and consequently the postpeak response obtained with the present model applies only to specimen sizes approximately the same as those tested. But calculations in the postpeak softening range can be made using some form of a localization limiter, for which the nonlocal theory is adopted here.

NUMERICAL STUDIES WITH NONLOCAL MICROPLANE MODEL

The present microplane model has been combined with the nonlocal theory, and the microplane finite-element program has been generalized for the nonlocal behavior. This makes it possible to model the size effects, which were investigated in the previous studies of the nonlocal smeared-cracking model and nonlocal microplane model (Bažant and Lin 1988; Bažant and Ožbolt 1990). Those studies dealt with tensile cracking and fracture. The present microplane model is more general and has been partly verified

for more general stress conditions. We are interested in applying it to nontensile failures. We explore a set of experiments available in the literature, those of van Mier (1984), dealing with uniaxial compressive failures of prisms of the same square section (100 × 100 mm) but different heights (50, 100, and 200 mm). These tests, strictly speaking, do not show what is understood as the size effect, because the specimens were not geometrically similar. Van Mier's tests show that the postpeak descending stress-strain diagram becomes steeper as the specimen height (length) (or the height-to-width ratio, slenderness) is increased.

Fig. 8 shows the three finite-element meshes used. Meshes A, B, and C correspond to van Mier's specimens 15A1-5 (height h = 50 mm), 10B1-3 (h = 100 mm), and 10B2-2 (h = 200 mm): They consist of 25 four-node isoparametric finite elements with 2 × 2 Gaussian integration points. The plane stress condition is assumed. The boundary conditions on the loaded sides are a sliding (frictionless) constraint in the x-direction. The load is introduced by prescribing uniform nodal displacements along the loaded side. The material parameters are the same as those indicated for the simulation of van Mier's cyclic uniaxial compressive test (Table 1). The characteristic length l is assumed to be $l = 3d_a = 3 \times 16$ mm = 48 mm (d_a is maximum aggregate size). The finite-element calculations are done not only with nonlocal averaging, but also without it.

The calculated load-displacement curves are compared to van Mier's data in Fig. 9(a). The load-displacement curves for both local and nonlocal calculations are almost the same in the cases of h = 50 and 100 mm, and they both agree with the experiments well. However, in the case of h = 200 mm, the maximum load value for the local calculation is too small, while the nonlocal calculation predicts the maximum well. Generally, the numerical convergence of the load-step iterations in the local calculations has not been good, although for the nonlocal calculations it has been very good. The reason is spurious strain localization in the case of local calculations; the nonlocal calculations do not have such a problem, as shown later.

Fig. 10 shows the distributions of strain ε_{xx} (lateral strain) at maximum load ($P = P_{max}$) for all the meshes; Fig. 10(a–c) are the nonlocal calculations, and Fig. 10(d–f) are the local calculations (here and in Figs. 11–13).

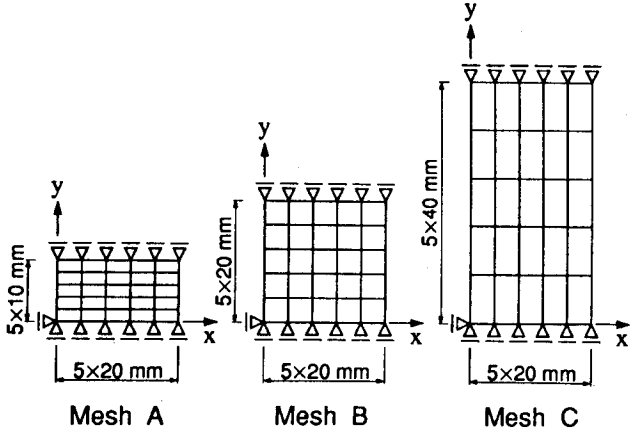

FIG. 8. Finite-Element Meshes for van Mier's (1974) Specimens

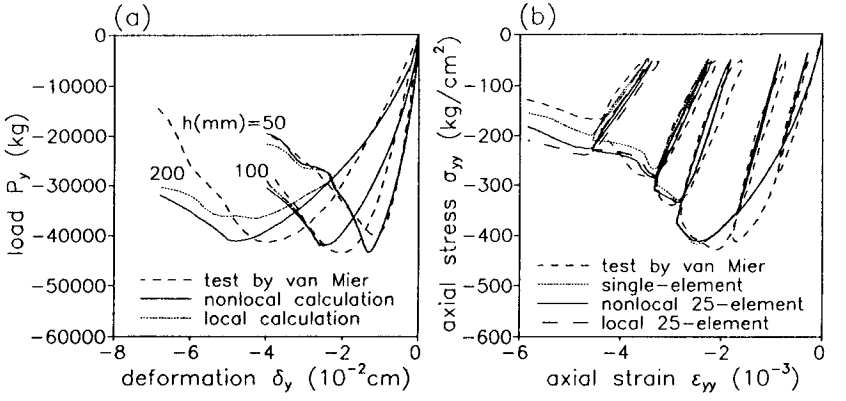

FIG. 9. (*a*) Comparison with van Mier's (1984) Tests on Effect of Height-to-Width Ratio; (*b*) Comparison with Cyclic Uniaxial Compressive Test by van Mier (1984) (Nonlocal 25-Element Calculation, Local 25-Element Calculation and Single Element Calculation)

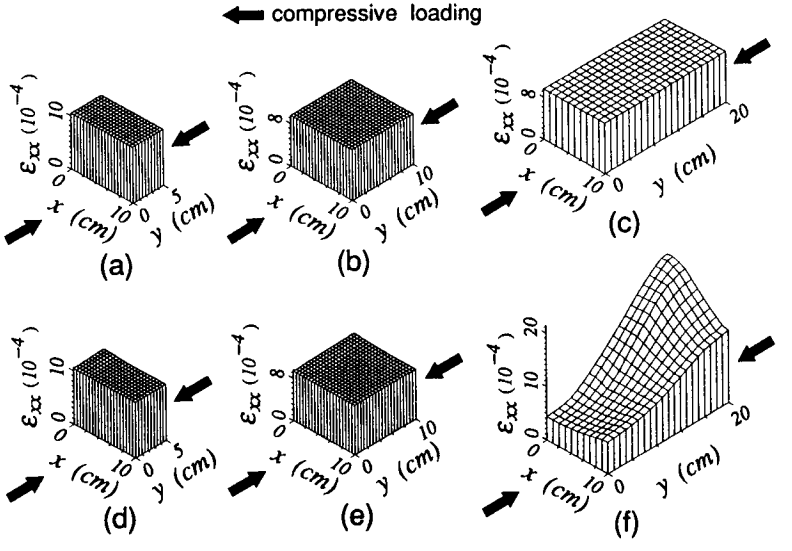

FIG. 10. Calculated Lateral Strain Distributions ε_{xx} at Maximum Load P_{max} for van Mier's (1984) Tests: (*a*)–(*c*) Nonlocal Calculations; (*d*)–(*f*) Local Calculations

There are only small differences between the distributions for nonlocal and local calculations for the heights h = 50 and 100 mm, but for h = 200 mm the strain distributions are very different, the strain field for the local calculation tends to localize. Fig. 11 shows the ε_{xx} distributions at postpeak load $P = 0.7P_{max}$ for all the meshes [the strain scale of Fig. 11(f) is different from the others]. A large strain localization occurs in the local case for h = 200 mm [Fig. 11(f)]; in the nonlocal case there is no pronounced localization, only a gradual strain distribution [Fig. 11(c)]. The localization ob-

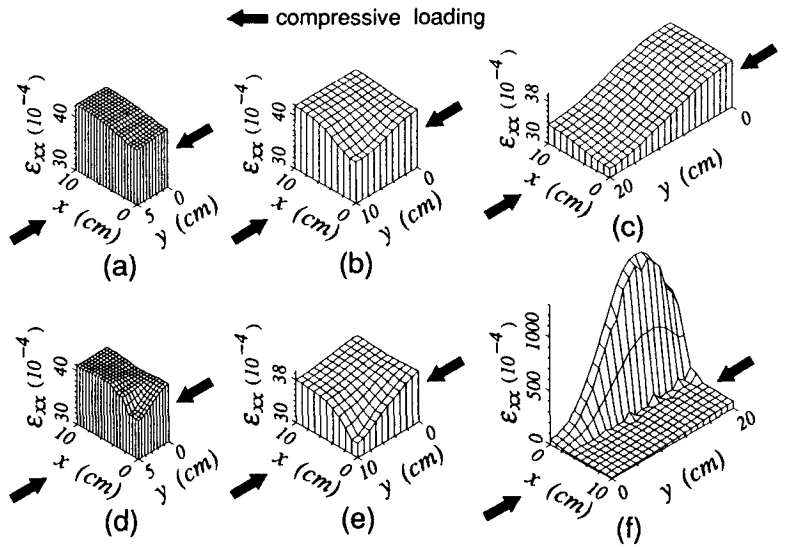

FIG. 11. Calculated Lateral Strain Distributions ε_{xx} at Load on Softening Regime ($P = 0.7P_{max}$) for van Mier's (1984) Tests: (a)–(c) Nonlocal Calculations: (d)–(f) Local Calculations

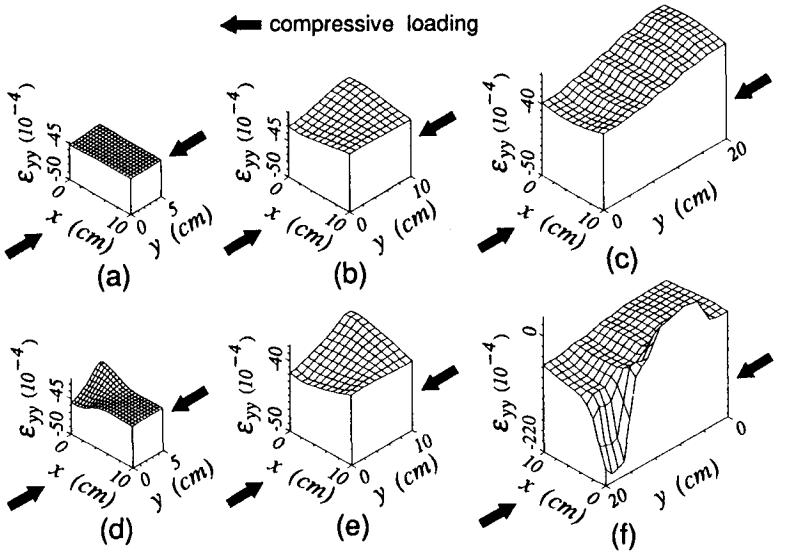

FIG. 12. Calculated Compressive Axial Strain Distributions ε_{yy} at Load on Softening Regime ($P = 0.7P_{max}$) for van Mier's (1984) Tests: (a)–(c) Nonlocal Calculations; (d)–(f) Local Calculations

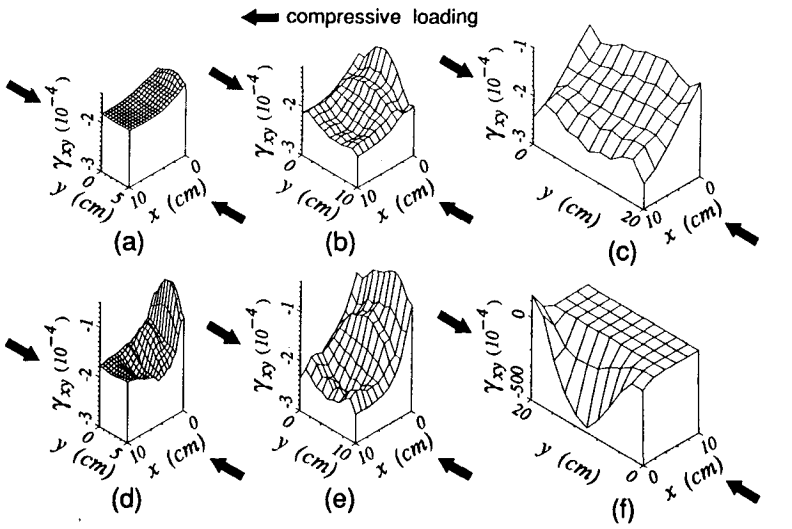

FIG. 13. Calculations Shear Strain Distributions γ_{xy} at Load on Softening Regime ($P = 0.7P_{max}$) for van Mier's (1984) Tests: (a)–(c) Nonlocal Calculations: (d)–(f) Local Calculations

tained in the local case seems to be spurious, due to numerical problems, which is indicated by poor numerical convergence and the fact that localization is seen to occur in only a single element band at $x = 0$ to 2 cm. Comparing the nonlocal and local cases for the heights $h = 50$ and 100 mm, the local case always gives a stronger localization than the nonlocal case.

Fig. 12 shows the distributions of ε_{yy} (compressive axial strain) at postpeak load $P = 0.7P_{max}$ for all the meshes [the strain scale of Fig. 12(*f*) is different from the others]. We can observe the same phenomena as in the case of ε_{xx}. Fig. 13 compares the distributions of shear strain γ_{xy} at postpeak load $P = 0.7P_{max}$, for all the meshes [the strain scale of Fig. 13(*f*) is different from the others]. At the maximum load, there are almost no shear strains in all the cases except the local case of $h = 200$ mm, in which the shear strains are localized. However, in Fig. 13 for the softening response the shear strains in all the cases are relatively large compared to those at the maximum load, especially in the local case for $h = 200$ mm [Fig. 13(*f*)]. The shear strain localization tends to increase with the mesh sizes, and the localization is more pronounced for the local cases.

To summarize the comparisons in Figs. 10–13, the nonlocal calculations always yield numerically stable solutions regardless of the specimen height or the element size; and the local calculations yield spurious localizations and poorer convergence when specimens much larger than l are analyzed. The nonlocal results of course do not represent the actual microstrains but macroscopically smoothed (averaged) strains.

The aforementioned strain distributions reveal differences in the failure mechanisms for different specimen heights. The first stage of damage is characterized by splitting cracks in the direction of compressive axis, as revealed by large values of the calculated lateral strains ε_{xx} in Figs. 10 and 11. After the peak load, the shear strains γ_{xy} increase markedly and tend to localize; prior to the peak load there is almost no shear strain. The shear

localization is more intense when the specimen height is larger. Since the shear localization represents local failure and may lead to buckling of the material strips between the splitting cracks, the load-carrying capacity of the specimens with larger height decreases at an earlier stage of the softening regime than for the specimens with smaller height. According to experimental observations, uniaxial compressive specimens without friction under the loading platens usually do not fail by shear bands but by axial splitting. The final failure probably occurs by snap-through buckling of the material strips between the splitting cracks. These experimental facts are consistent with the present analytical results.

In the present calculations, the finite elements were relatively large compared with the specimen sizes and with the characteristic length l. Thus it might be that the element subdivision might not be sufficiently fine to represent the deformation field, and especially the shear band localization mode. Calculations with finer meshes are desirable.

In this study, the characteristic length l is fixed as $l = 3d_a$, which is the approximation suggested for the crack-band theory (Bažant and Oh 1983). The effect of changing l has not been explored, but the estimate $l = 3d_a$ is certainly a crude guess and the value l would better be identified by fitting of more extensive test data on the effects of both the height-to-width ratio and the specimen size for the same height-to-width ratio. But such comprehensive test data are lacking.

It is interesting to compare the cyclic calculation results using the nonlocal and local microplane models. Van Mier's (1984) cyclic uniaxial compressive test data for the specimen with height $h = 100$ mm were fitted in Fig. 4 with a single finite element, and mesh B (100×100 mm) is then used along with the same material parameters given in Table 1. Fig. 9(b) shows the calculated stress-strain curves along with the previous result using a single finite element, for comparison (the load-displacement data were converted into average stress-strain data for the total specimen height). The differences between the nonlocal 25-element calculation, the local 25-element calculation, and the single-element calculation are seen to increase with increasing strain. However, the differences between the strain (ε_{xx}, ε_{yy}, and γ_{xy}) distributions of the nonlocal and local 25-element calculations are very small compared to differences in the results for different specimen heights.

CONCLUSIONS

1. The previously formulated nonlocal microplane model for concrete is improved to describe the cyclic and rate-dependent behaviors. By contrast with the previous microplane model, the normal strain component on the microplane is not split into its volumetric and deviatoric parts; instead, the lateral normal strains are considered. The penalty is that the full range of Poisson's ratio cannot be covered, but the Poisson ratio values typical for concrete can be obtained. Furthermore, instead of one shear strain resultant on the microplane, the shear strain is represented by two shear components in the directions of two in-plane coordinates. This approach appears to eliminate some possibly unrealistic features of the calculated response on the microplanes (although this question cannot be decided by direct experimental observations).

2. The response of the normal strain component on the microplane is varied from hydrostatic response to plastic response and to softening response as a function of lateral normal strain on the same microplane. As before, the microplane strains are the resolved components of the macrostrain (kinematic constraint), but the response of the shear component is made to depend on the resolved normal component of the macroscopic stress tensor on the same microplane (which represents a static constraint). This allows it to represent more closely the physical concept of friction. The values of peak stress, strain at peak, ductility, and the postpeak shape of the descending stress-strain curve for the microplane components, can be used to control the macroscopic response in an easily understandable manner. In the case of monotonic loading tests, 10 microplane material parameters have to be identified by fitting test data.

3. To model rate dependence, a Maxwell-type rheologic model consisting of a linear viscous element with a constant relaxation time coupled in series with an elastoplastic-fracturing element is adopted for each microplane strain component. The exponential algorithm previously developed for creep (and previously also applied to a different microplane model) is adapted to this formulation to calculate the response for each microplane component in the time steps of numerical integration.

4. Nonlinear unloading-reloading hysteresis rules are developed for each elastoplastic-fracturing element using the concept of back-stress and objective-stress. Furthermore, cyclic rules are set up for the overall response of the generalized Maxwell model or each microplane component, covering both the tensile and compressive stress ranges and general strain histories.

5. The present microplane model describes reasonably well the existing test data from cyclic uniaxial compressive and tensile tests, triaxial compressive tests, and the strain-rate effect in uniaxial compressive tests. The model also realistically describes the strain-softening, damage processes, the hysteretic properties during unloading and reloading, the confinement effect on the transition from softening to hardening, and the hydrostatic response.

6. A nonlocal generalization of the present microplane model can well represent localization behavior and the effect of height-to-width ratio on uniaxial compressive softening. Generally, the numerical convergence of the finite-element calculations is not good for the local model, but is good for the nonlocal model.

ACKNOWLEDGMENT

The present results have been obtained under a joint research program between Shimizu Corporation, Tokyo, and Northwestern University. The first author wishes to thank Shimizu Corporation for giving him the opportunity to conduct this research at Northwestern University.

APPENDIX. REFERENCES

Bažant, Z. P., and Oh, B. H. (1983). "Crack band theory for fracture of concrete." *Matériaux et Constructions*, Paris, France, 16(93), 155–177.

Bažant, Z. P., and Oh, B. H. (1986). "Efficient numerical integration on the surface of a sphere." *Zeitschrift für Angewandte Mathematik und Mechanik*, Leipzig, Germany, 66(1), 37–49.

Bažant, Z. P., and Ožbolt, J. (1990). "Nonlocal microplane model for fracture, damage, and size effect in structures." *J. Engrg. Mech.*, ASCE, 116(11), 2485–2505.

Bažant, Z. P., and Prat, P. C. (1988a). "Microplane model for brittle-plastic material: I. Theory." *J. Engrg. Mech.*, ASCE, 114(10), 1672–1688.
Bažant, Z. P., and Prat, P. C. (1988b). "Microplane model for brittle-plastic material: II. Verification." *J. Engrg. Mech.*, ASCE, 114(10), 1689–1702.
Carol, I., Bažant, Z. P., and Prat, P. C. (1992). "New explicit microplane model or concrete: Theoretical aspects and numerical implementation." *Int. J. of Solids and Struct.*, 29(9), 1173–1191.
Dilger, W. H., Koch, R., and Kowalczyk, R. (1984). "Ductility of plain and confined concrete under different strain rates." *ACI J.*, 81(1), 73–81.
Green, S. J., and Swanson, S. R. (1973). "Static constitutive relations for concrete." *Rep. No. AFWL-TR-72-2*, Air Force Weapons Laboratory, Kirtland Air Force Base.
Hasegawa, T., and Bažant, Z. P. (1993). "Nonlocal Microplane concrete model with rate effect and load cycles. I: General formulation." *J. Mat. in Civ. Engrg.*, ASCE, 7(3), 372–393.
Karsan, D., and Jirsa, J. O. (1969). "Behavior of concrete under compressive loadings." *J. Struct. Div.*, ASCE, 95(12), 2543–2563.
Ožbolt, J., and Bažant, Z. P. (1991). "Cyclic microplane model for concrete." *Proc. Int. RILEM/ESIS Conf. on fracture processes in brittle disordered materials: concrete, rock, ceramics*, Chapman & Hall, London, England, 639–650.
Reinhardt, H. W., and Cornelissen, H. A. W. (1984). "Post-peak cyclic behaviour of concrete in uniaxial tensile and alternating tensile and compressive loading." *Cement and Concrete Res.*, 14(2), 263–270.
van Mier, J. G. M. (1984). "Strain-softening of concrete under multiaxial loading conditions," PhD thesis, Eindhoven University of Technology, Eindhoven, The Netherlands.
Willam, K., Hurlbut, B., and Sture, S. (1986). "Experimental and constitutive aspects of concrete failure." *Finite element analysis of reinforced concrete structures*, C. Meyer and H. Okamura, eds., ASCE, New York, N.Y., 226–254.